Supporting Information

V doping coupled H_2O_2 pre-oxidation synergistically promote NiCo-LDH for urea oxidation assisted hydrogen production

Jiawei Guo, Heng Zhang, Yusen Yang, Min Wei, Hui Zhang*

State Key Laboratory of Chemical Resource Engineering, Beijing University of Chemical Technology, Beijing 100029, China.

*Corresponding author: Hui Zhang

Tel.: +8610 64425872;

Fax: +8610 64425385;

E-mail: zhanghui@mail.buct.edu.cn; huizhang67@gst21.com

Experiment

1. Chemical reagents

The experimental reagents used are all analytically pure, and no further purification is required before use. $Ni(NO_3)_2 \cdot 6H_2O$, $Co(NO_3)_2 \cdot 6H_2O$, VCl_3, $CO(NH_2)_2$ H_2O_2, RuO_2 and 20% Pt/C were obtained from Aladdin., Acetone (C_3H_6O, ≥99.9%) and ethanol (C_2H_5OH, ≥99.9%) were purchased from Thermo Fisher Scientific, and nickel foam (NF, 95% purity) was purchased from Saibo Company. The NF (cut into a size of 4 cm × 4 cm) was ultrasonically treated with acetone, 1 M hydrochloric acid, deionized water and absolute ethanol for 15 minutes respectively, to remove oxides on the surface, and then dried at 80°C in vacuum for 2 h.

2. Experimental

2.1 Synthesis of NiCoV$_x$-LDH/NF composites.

$Ni(NO_3)_2 \cdot 6H_2O$ (1.0 mmol), $Co(NO_3)_2 \cdot 6H_2O$ (0.5 mmol), VCl_3 (0.5 mmol) and $CO(NH_2)_2$ (10 mmol) were dissolved in deionized water (40 mL) and ethanol (40 mL). Then the solution and a clean nickel foam (4 cm × 4 cm) were transferred to 100 mL polytetrafluoroethylene lined stainless steel autoclave, and reacted in an oven at 120°C for 12 h, after natural cooling to room temperature, rinsed with deionized water five times (5 min each time) and freeze-dried to obtain NiCoV$_{1.0}$-LDH/NF (the mole ratio of V: Co is 1.0). Other catalysts were prepared by controlling the amounts of VCl_3 (0, 0.25 and 0.75 mmol), and denoted as NiCo-LDH/NF, NiCoV$_{0.5}$-LDH/NF, and NiCoV$_{1.5}$-LDH/NF, respectively.

2.2 Synthesis of NiCoV$_{1.0}$-LDH/NF-y composites.

The mixture of $Ni(NO_3)_2 \cdot 6H_2O$ (1.0 mmol), $Co(NO_3)_2 \cdot 6H_2O$ (0.5 mmol), VCl_3 (0.5 mmol) and $CO(NH_2)_2$ (10 mmol) was dissolved in deionized water (40 mL) and ethanol (40 mL). A transparent solution was obtained by continuous stirring and ultrasonic dissolution. Then the 3 wt% H_2O_2 (100 μL) is slowly dripped into the above solution. The obtained solution and a clean nickel foam (4 cm × 4 cm) were transferred to 100 mL polytetrafluoroethylene lined stainless steel autoclave, and then treated at 120°C for 12 hours in an oven. After natural cooling to room temperature, the electrocatalyst was obtained by freeze-drying the precipitate, which was cleaned by deionized water for five times (5 min each time) and name as NiCoV-LDH/NF-100. Other catalysts were prepared by controlling the addition of H_2O_2 (50 and 200 μL) and were denoted as NiCoV$_{1.0}$-LDH/NF-50 and NiCoV$_{1.0}$-LDH/NF-200, respectively.

2.3 Synthesis of NiCoV$_{1.0}$-LDH/rGO/NF-100 composites.

Firstly, the rGO modified Ni foam (rGO/NF) was pre-prepared by referring to our previous work. [1-3] 60

mL of 0.5 mg/mL GO sol was ultrasonicated for 20 min, and then added with 30 mg of citric acid (CA) for further ultrasonication for 5 min to obtain the CA-GO suspension. Subsequently, the obtained CA-GO suspension and two pieces of cleaned NF were placed into a 100 mL autoclave and treated at 120°C for 5 h. Until autoclave cooled off naturally, followed repeatedly rinsed with deionized water to wash away the rGO weakly attached on the surface and in the pores of the NF skeleton, and freeze-dried to obtain rGO/NF. Then, the same volume of the above precursor solution was added to an autoclave containing a piece of rGO/NF, and the reaction was carried out under the same conditions. The obtained product was denoted as $NiCoV_{1.0}$-LDH/rGO/NF-100.

2.4 Commercial catalyst.

RuO_2 (25 mg) was dispersed in a 1 mL mixed solution (770 μL water, 30 μL 5 wt % Nafion solution, and 200 μL ethanol), followed by sonication to obtain a catalyst ink. The catalyst ink (100 μL) was then dropcast on the surface of Ni foam (1 cm × 1 cm), which was dried at 80°C for 4 h. The catalyst loading was all ca. 2.5 mg cm^{-2}.

The 20% Pt/C electrode was prepared by the similar method mentioned above.

3. Material Characterization

The X-ray diffraction (XRD) patterns were recorded on the Shimadzu XRD-6000 diffractometer with Cu-Kα radiation (λ = 0.15418 nm, 30 mA, 40 kV) in the 2θ scanning range of 3-80º, at a scanning speed of 10°/min. The scanning electron microscope (SEM) images were obtained on Hitachi S-3500N operating at 20 kV. High-resolution transmission electron microscope (HRTEM) images were obtained on JEM 2010 instrument operating at 200 kV. The Raman spectra were obtained with a Jobin Yvon Hodiba Raman spectrometer model HR800 using a 532 nm line of Ar^+ ion laser as the excitation source at room temperature. X-ray photoelectron spectroscopy (XPS) was recorded on the VG Escalab-250 (Al Kα radiator). Thermogravimetric analysis (TGA) was performed on a Mettler-Toledo TGA/DSC 1/110 ST thermal analyzer, and the sample was heated from 25 to 700 °C under N_2 flow (~50 mL/min). X-ray absorption fine structure spectroscopy (XAFS) was measured at the beamline 1W1B of the Beijing Synchrotron Radiation Facility (BSRF), Institute of High Energy Physics (IHEP), Chinese Academy of Sciences (CAS). XAFS data were collected with an electron beam energy of 2.5 GeV and a beam current of 250 mA with a fixed-exit double-crystal Si(111) monochromator. The raw data were analyzed performed with the IFEFFIT software package, according to standard data analysis procedures.

4. Electrochemical characterization

The electrochemical performance tests in this paper were all completed on the CHI660D electrochemical workstation. The electrolytes used in UOR and HER experiments were 1 M KOH + 0.3 M and 1 M KOH, respectively. In the case of three electrodes, the working electrode was the as-prepared catalyst (the submerged area is 1 cm × 1 cm), and the Hg/HgO electrode was used as the reference electrode. In UOR reaction, the Pt sheet is used as the counter electrode, while in HER reaction, the carbon rod is used as the counter electrode. N_2 must be introduced for 20 min before all tests began, and all potentials were measured according to the Nernst Eq. (S1). and converted to reversible hydrogen electrode.

$$E_{RHE} = E_{Hg/HgO} + 0.059 \, pH + 0.098 \, V \tag{S1}$$

The electrocatalytic activity of all electrodes was evaluated using linear sweep voltammetry (LSV) at a scanning rate of 5 mV s^{-1}. The Tafel slope is derived from the polarization curve and fitted according to the Eq. (S2):

$$\eta = a + b \log j \tag{S2}$$

Where η is the overpotential, j is the measured current density, b is the Tafel slope, and a is the constant. C_{dl} was measured from the double layer charge curve by CV in the small potential range of 0.1 - 0.2 V relative to Hg/HgO electrodes at scan rates of 10, 20, 30, 40 and 50 mV s^{-1}. At 0.15 V, $\Delta j = (j_a - j_c)$ has a linear relation with the scanning rate of Hg/HgO electrode, and the linear slope is twice that of the double layer capacitance. The EIS applies an AC voltage of 5 mV at a frequency of 10 kHz to 0.01 Hz.

The ECSA of the catalyst was calculated according to the following Eq. (S3):

$$ECSA = C_{dl}/C_s \tag{S3}$$

where C_s is specific capacitance in an alkaline electrolyte for Ni foam ($C_s = 0.040 \, mF \, cm^{-2}$).

In order to further explain the intrinsic activity of the catalysts, the turnover frequency (TOF) at a certain overpotential was calculated according to the Eq. (S4 and S5):

$$UOR: TOF = \frac{j \times A}{6 \times F \times m} \tag{S4}$$

$$HER: TOF = \frac{j \times A}{2 \times F \times m} \tag{S5}$$

where j is current density at a certain overpotential (A cm^{-2}), A is surface area of the working electrode (1 cm^2), F is Faraday constant (96485 C mol^{-1}) and m is concentration of active sites in the catalyst (mol cm^{-2}).

The Faradaic efficiency (FE) is calculated according to the following relationship:

$$FE = \frac{2F \times n_{H2}}{Q} = \frac{2F \times n_{H2}}{It} \tag{S6}$$

Where n_{H2} is the amount of hydrogen (mol), F is the Faraday constant (96500 C/mol), Q is the total amount of charge passed through the cell (C), I is the current, and t is the collection time.

5. DFT + U calculation

The present first principle Density functional theory (DFT) calculations are performed by Vienna *Ab initio* Simulation Package (VASP) with the projector augmented wave (PAW) method. The exchange-functional is treated using the generalized gradient approximation (GGA) of Perdew-Burke-Ernzerhof (PBE) functional. The DFT + D3 method developed by Grimme was employed to treat the Van der Waals interactions. The Ueff (U-J) values of 6.2 eV, 3.32 eV and 3.25 eV were applied for Ni, Co and V 3d states. The energy cutoff for the plane wave basis expansion was set to 500 eV and the force on each atom less than 0.05 eV/Å was set for convergence criterion of geometry relaxation. The self-consistent calculations apply a convergence energy threshold of 10-5 eV. To avoid the periodical interactions, a ~15 Å vacuum space was added in *z*-direction. The Brillouin zone integration was performed using $3 \times 3 \times 1$ Monkhorst and Pack *k*-point sampling through all the computational process.

The transition state (TS) searches are performed using the Dimer method in the VTST package. The final force on each atom was < 0.05 eV Å^{-1}. The TS search is conducted by using the climbing-image nudged elastic band (CI-NEB) method to generate initial guess geometries, followed by the dimer method to converge to the saddle points.

The free energy of the HER step was calculated by the equation: $\Delta G = \Delta E_{DFT} + \Delta E_{ZPE} - T\Delta S$, where ΔE_{DFT} was the DFT electronic energy difference of each step, ΔE_{ZPE} and ΔS are the correction of zero-point energy and the variation of entropy, respectively, which were obtained by vibration analysis, T was the temperature (the value here was room temperature).
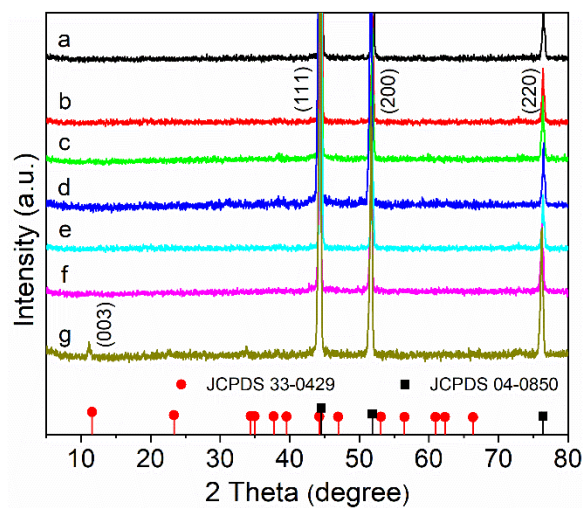
Fig. S1 XRD patterns of NiCoV$_{1.0}$-LDH/NF-y (a-c: y = 50, 100, 200), NiCoV$_x$-LDH/NF (d-f: x = 0.5, 1.0, 1.5) and NiCo-LDH/NF (g) composites.
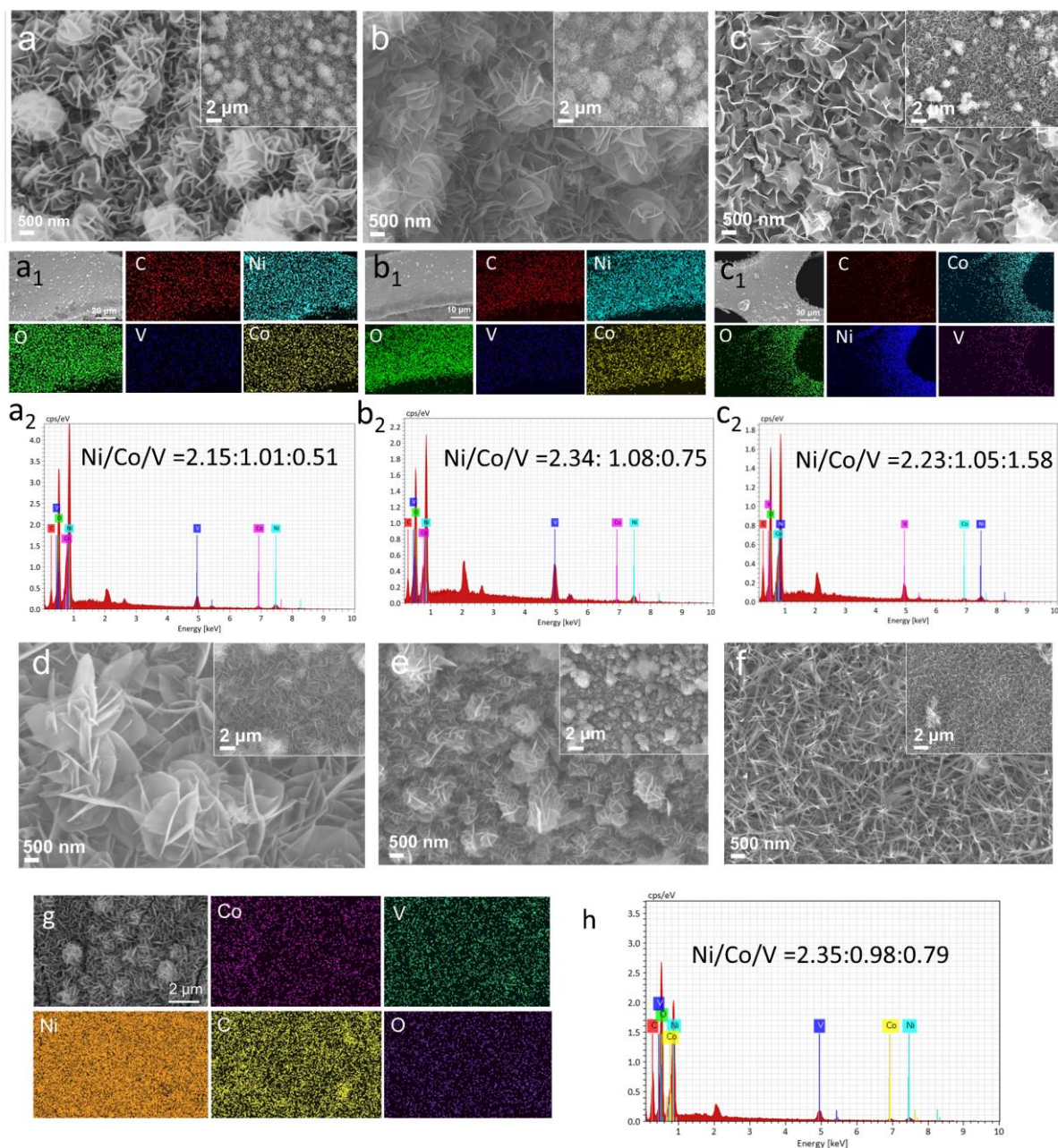
Fig. S2 SEM images (a-c), SEM-EDX elemental mappings (a$_1$-c$_1$) and SEM-EDS spectra (a$_2$-c$_2$) of NiCoV$_x$-LDH/NF (a-c: x = 0.5, 1.0, 1.5). SEM images of NiCoV$_{1.0}$-LDH/NF-y (d, e: y = 50, 200) and NiCo-LDH/NF (f). SEM-EDX elemental mapping (g) and SEM-EDS spectrum (h) of NiCoV$_{1.0}$-LDH/NF-100.

s
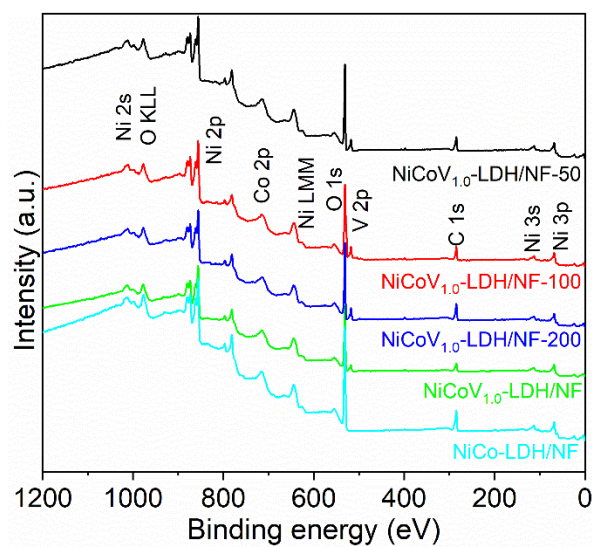
Fig. S3 Full XPS survey spectra of NiCoV$_{1.0}$-LDH/NF-y (y = 50, 100, 200), NiCoV$_{1.0}$-LDH/NF and NiCo-LDH/NF.
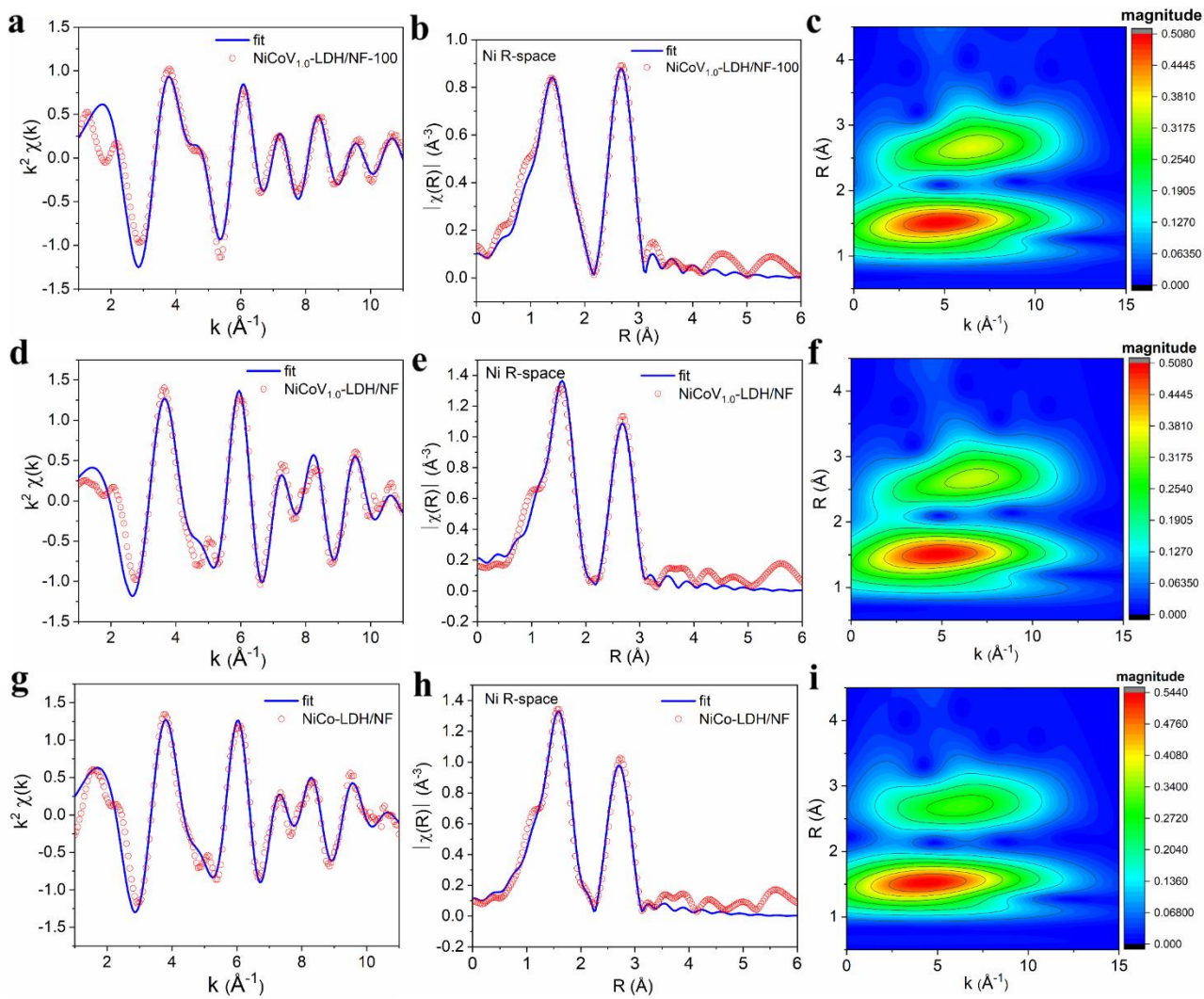
Fig. S4 Ni K-edge EXAFS (points) and fit (line) k^2 weighted k-space, k^2 weighted R-space, and the wavelet transform: (a-c) NiCoV$_{1.0}$-LDH/NF-100, (d-f) NiCoV$_{1.0}$-LDH/NF, (g-i) NiCo-LDH/NF.
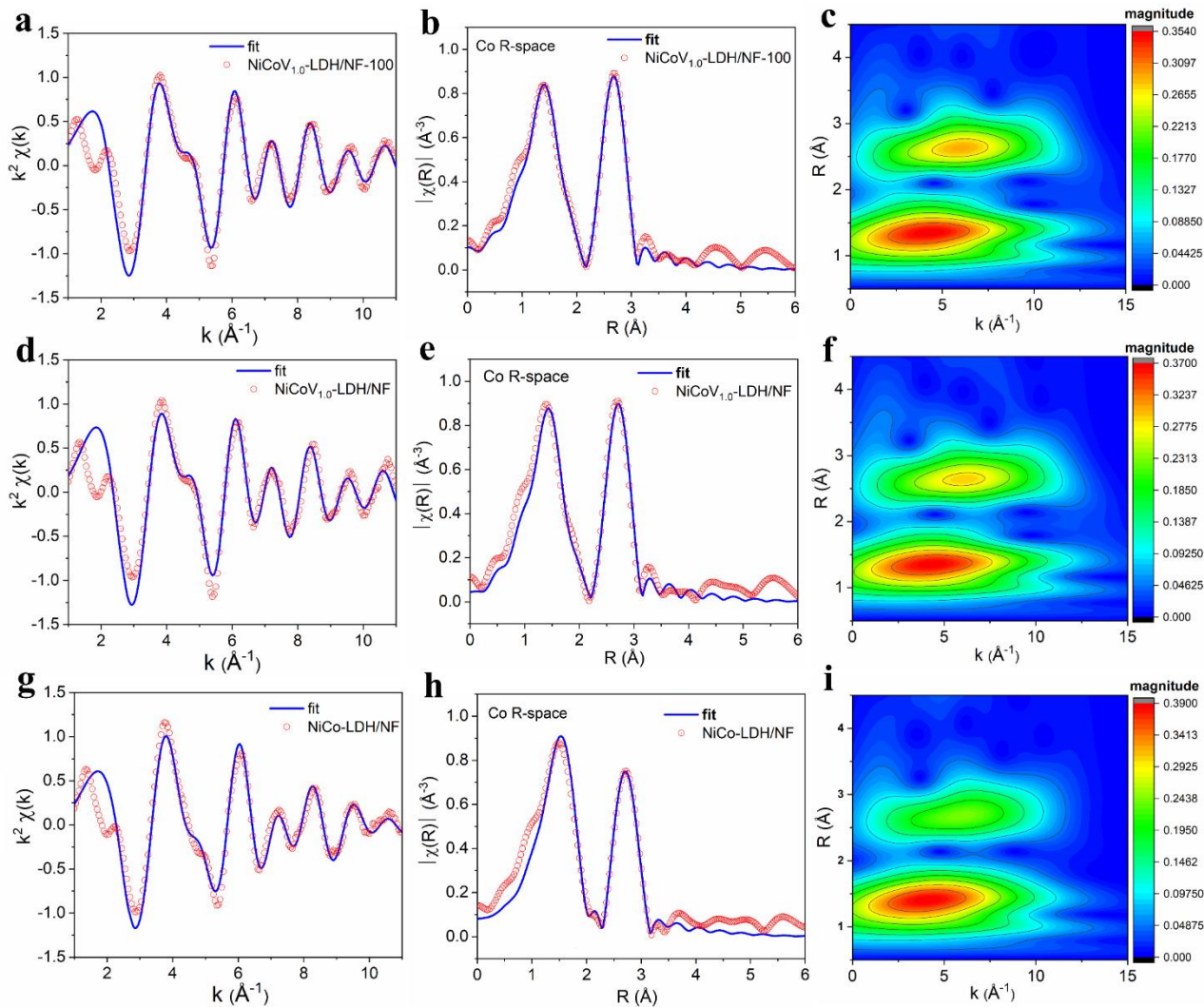
Fig. S5 Co K-edge EXAFS (points) and fit (line) k^2 weighted k-space, k^2 weighted R-space, and the wavelet transform: (a-c) $NiCoV_{1.0}$-LDH/NF-100, (d-f) $NiCoV_{1.0}$-LDH/NF, (g-i) NiCo-LDH/NF.
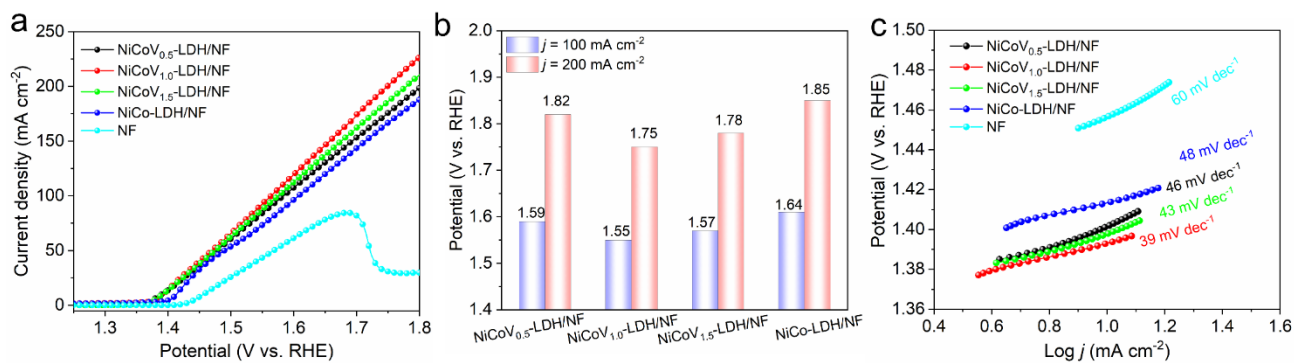
Fig. S6 (a) UOR polarization, (b) comparison of potentials at 100 and 200 mA cm^{-2}, (c) Tafel slopes of NiCoV$_x$-LDH/NF (x = 0.5, 1.0, 1.5), NiCo-LDH/NF and NF.
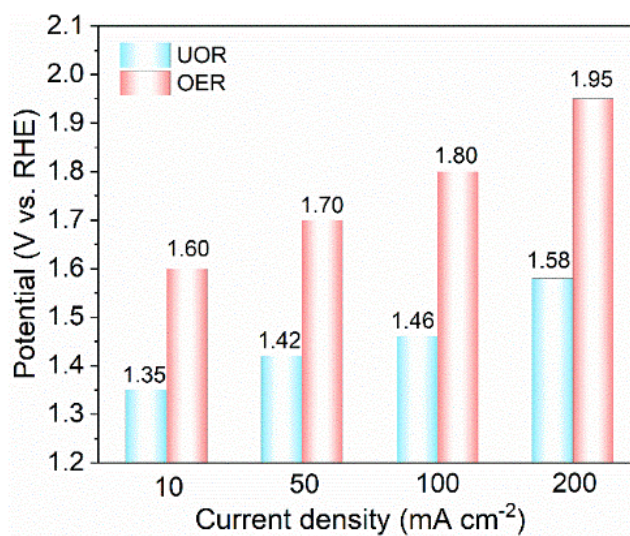
Fig. S7 Potentials of NiCoV$_{1.0}$-LDH/NF-100 needed to reach 10, 50, 100 and 200 mA cm^{-2} for UOR and OER.
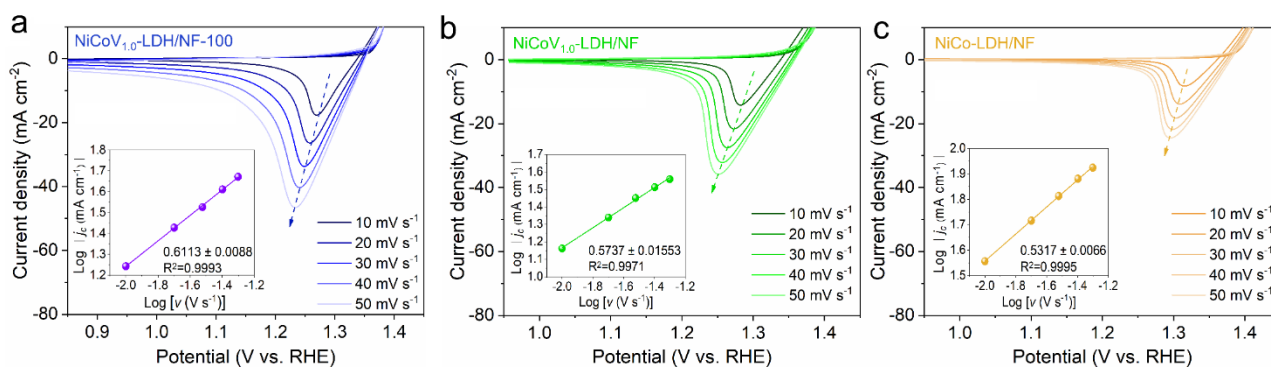
Fig. S8 Cyclic voltammograms at different scan rates. The inset is plot of the logarithm of cathodic peak current density (j_c) against the logarithm of scan rate (v). (a) NiCoV$_{1.0}$-LDH/NF-100, (b) NiCoV$_{1.0}$-LDH/NF, (c) NiCo-LDH/NF composites.

The cyclic voltammetry (CV) curve was used to determine the effect of scanning rate on the electrocatalytic oxidation of urea in NiCoV$_{1.0}$-LDH/NF-100 electrode. In general, the cathode current density (j_c) increases with the increase of scanning rate (v), and there is a power-law relationship between the peak cathode current density and scanning rate: $j_c = av^b$ [4]. The exponential b value of the redox process can be obtained by comparing the logarithm of the cathode peak current density with the logarithm of the scanning rate. In two limiting conditions: (i) when b = 0.5, it is a diffusion-controlled redox process; (ii) when b = 1, it is non-diffusion controlled capacitive behavior. As shown in Fig. S8, the cathode current density of NiCoV$_{1.0}$-LDH/NF-100 increased with increasing scan rate, and the logarithm of the peak cathode current density was linearly related to the logarithm of the scan rate, and b = 0.6113, indicating that UOR is an electrode process controlled by diffusion and surface capacitance. In addition, the b values of NiCoV$_{1.0}$-LDH/NF and NiCo-LDH/NF were 0.5737 and 0.5317, respectively, indicating that the electrode processes are similar to those of NiCoV$_{1.0}$-LDH/NF-100, which are both mixed-controlled electrode processes of diffusion and capacitance behavior.
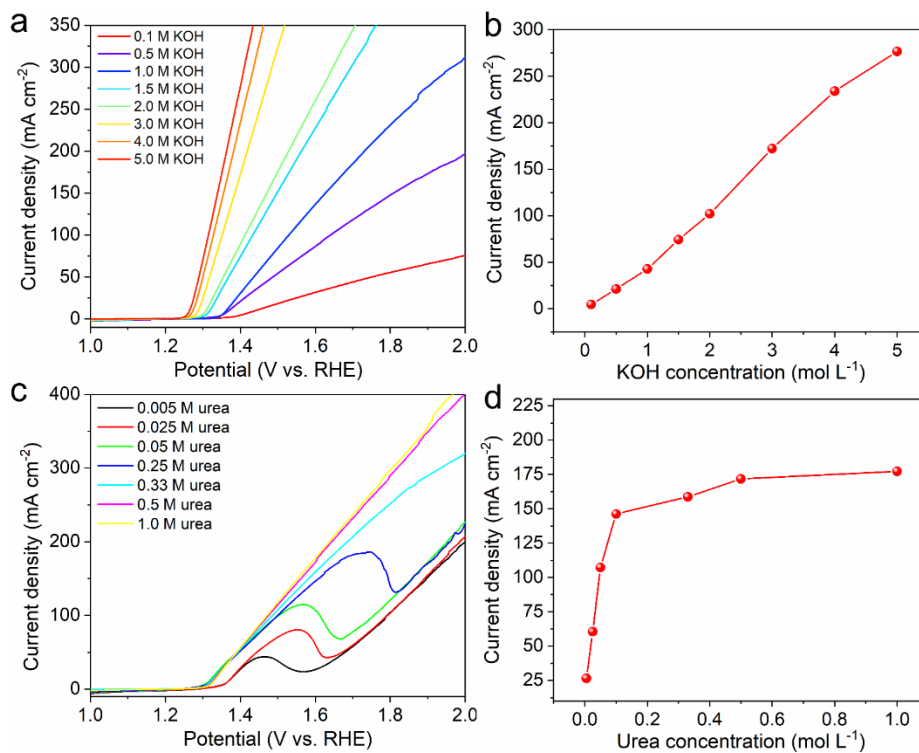
Fig. S9 NiCoV$_{1.0}$-LDH/NF-100 (a) LSV curves of different concentrations of KOH in 0.33 M urea; (b) LSV curves of urea with different concentrations in 1.0 M KOH. (c) Relation between current density and KOH at 1.4 V. (d) Relationship between current density and urea concentration at 1.6 V.
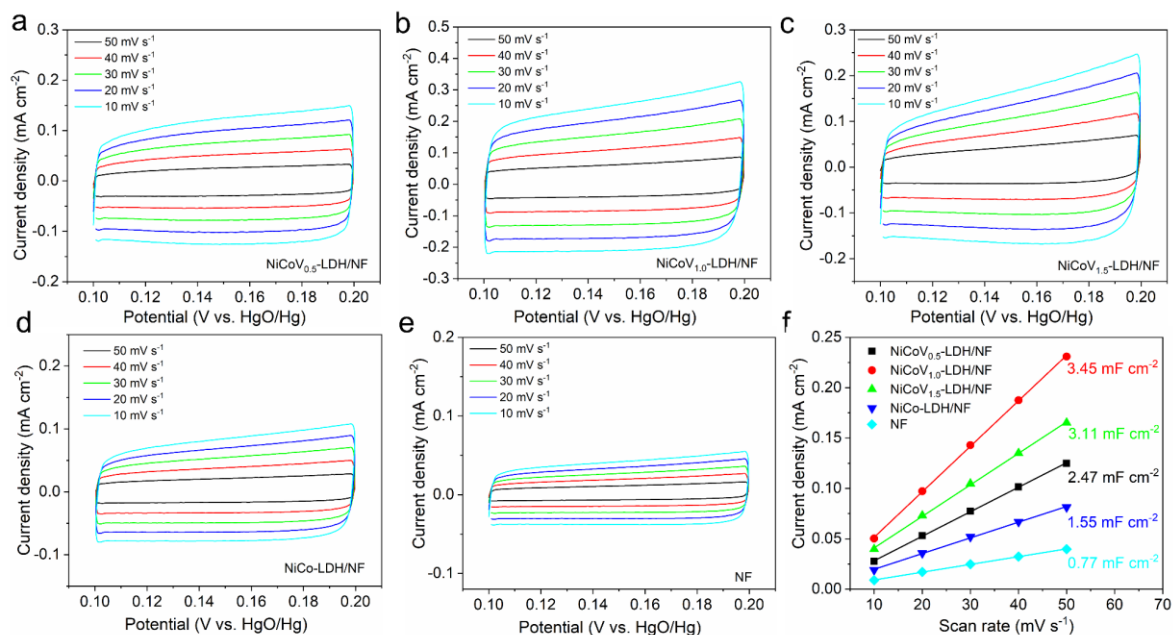
Fig. S10 (a-d) Cyclic voltammetry curves of NiCoV$_x$-LDH/NF (x = 0.5, 1.0, 1.5), NiCo-LDH/NF composites and bare NF at various scan rates in the region of 0.1 - 0.2 V vs. Hg/HgO in 1 M KOH + 0.33 M urea solution. (f) The current densities of NiCoV$_x$-LDH/NF (x = 0.5, 1.0, 1.5), NiCo-LDH/NF composites and bare NF plotted against different scan rates (10, 20, 30, 40, 50 mV s^{-1}).
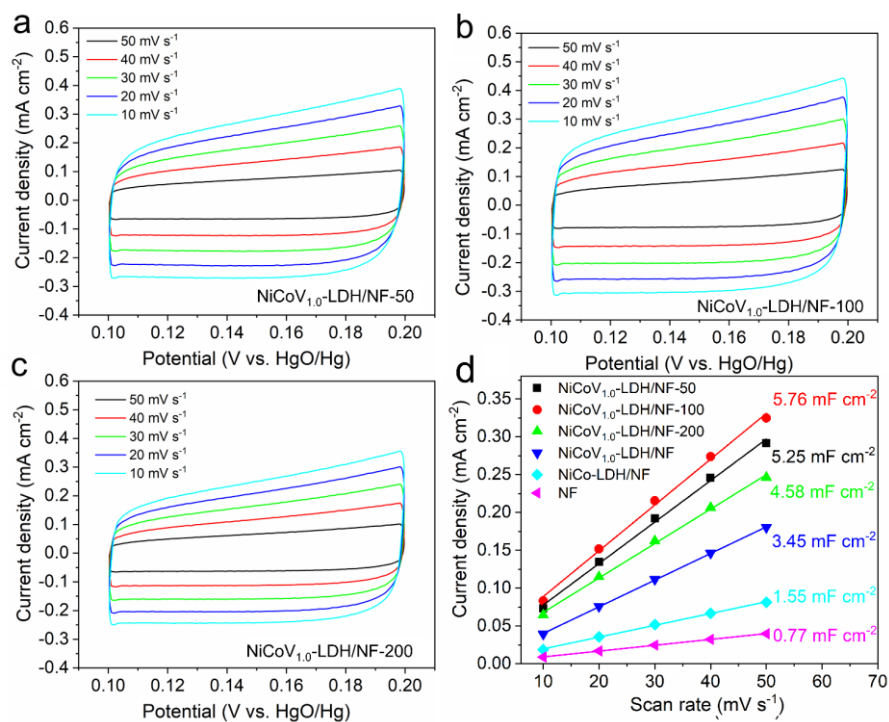
Fig. S11 (a-c) Cyclic voltammetry curves of the NiCoV$_{1.0}$-LDH/NF-y (y = 50, 100, 200) composites at various scan rates in the region of 0.1 - 0.2 V vs. Hg/HgO in 1 M KOH + 0.33 M urea solution. (d) The current densities of NiCoV$_{1.0}$-LDH/NF-y (y = 50, 100, 200), NiCoV$_{1.0}$-LDH/NF, NiCo-LDH/NF composites and bare NF plotted against different scan rates (10, 20, 30, 40, 50 mV s^{-1}).

14
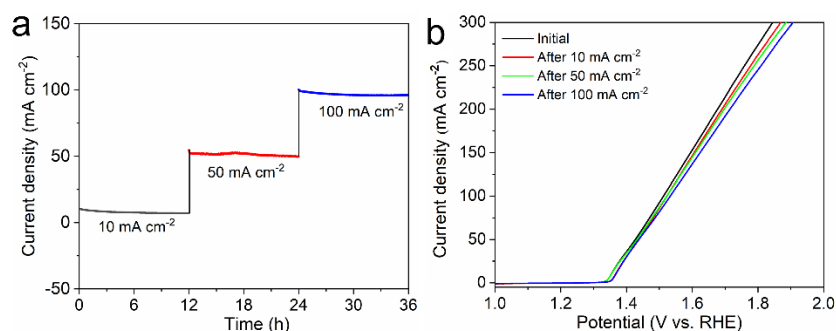
Fig. S12 (a) UOR stability test and (b) LSV comparison before and after stability test of NiCoV$_{1.0}$-LDH/NF-100 composite.
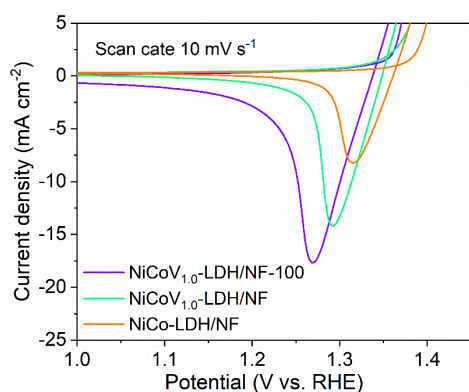
Fig. S13 CV curves for UOR of NiCoV$_{1.0}$-LDH/NF-100, NiCoV$_{1.0}$-LDH/NF and NiCo-LDH/NF composites at a scan rate of 10 mV s^{-1}.
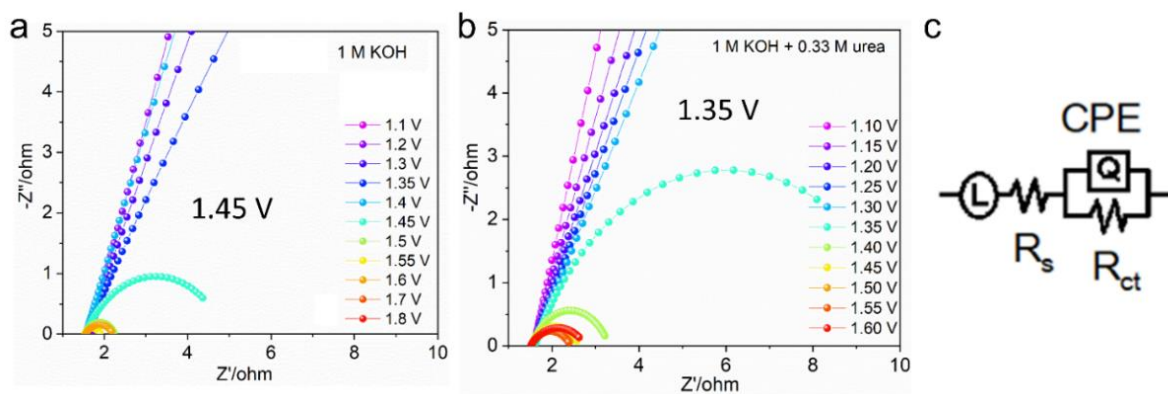
Fig. S14 In-situ Nyquist diagram in 1 M KOH (a) and 1 M KOH + 0.33 M urea (b) of NiCoV$_{1.0}$-LDH/NF-100 and corresponding fitting circuit diagram (c).
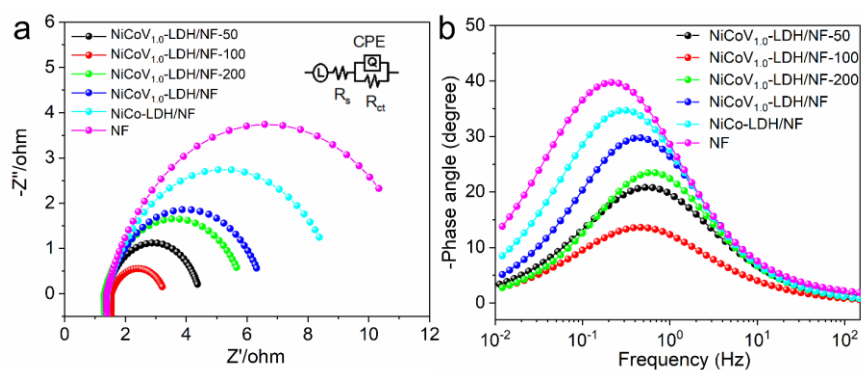
Fig. S15 (a) Nyquist diagram and (b) Bode diagram of NiCoV$_{1.0}$-LDH/NF-y (y = 50, 100, 200), NiCoV$_{1.0}$-LDH/NF, NiCo-LDH/NF and NF at 1.45 V in 1 M KOH + 0.33 M urea.
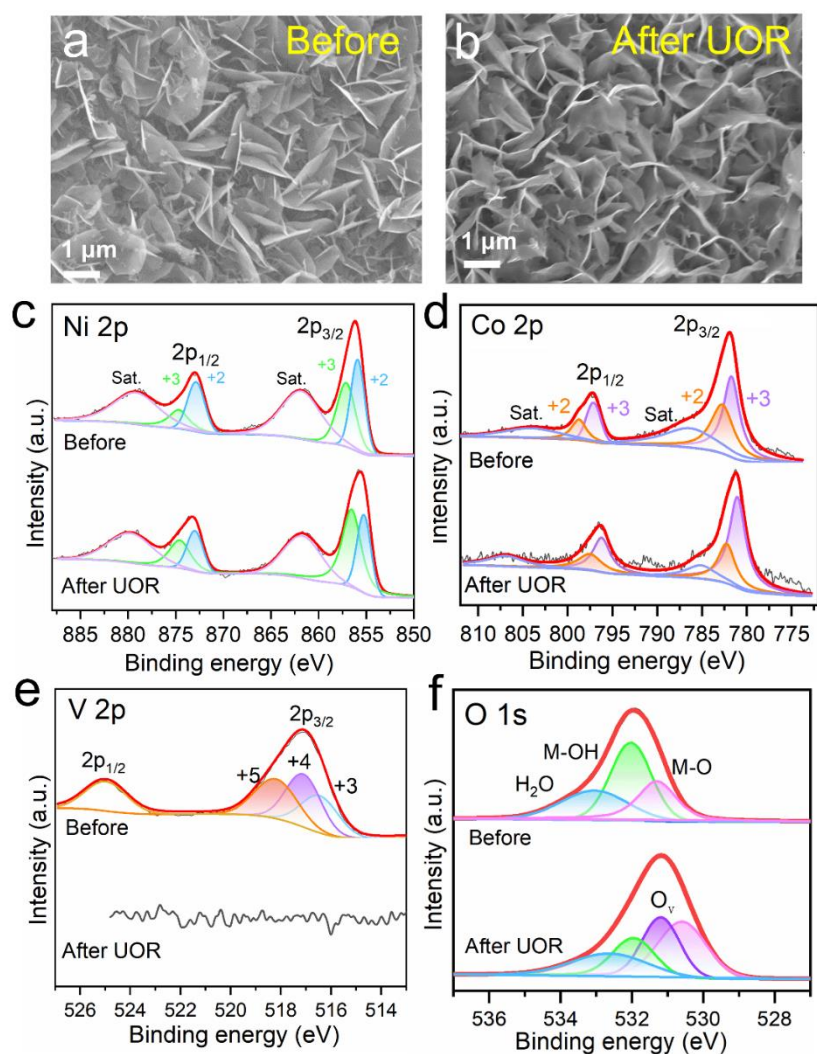
Fig. S16 (a-b) SEM comparison of NiCoV$_{1.0}$-LDH/NF-100 before and after UOR reaction. (c-f) Ni 2p, Co 2p, V 2p, C 1s and O 1s XPS spectra of NiCoV$_{1.0}$-LDH/NF-100 before and after UOR stability.
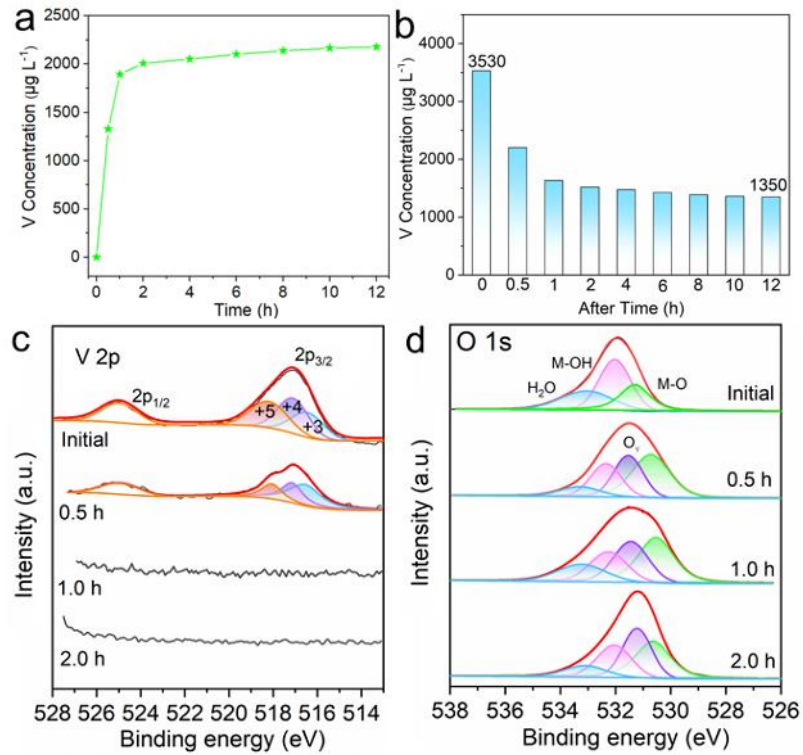
Fig. S17 (a) The dissolved V concentration in the electrolyte of NiCoV$_{1.0}$-LDH/NF-100 via ICP; (b) V concentration in NiCoV$_{1.0}$-LDH/NF-100 at different reaction time. (c-d) Comparison V 2p and O 1s XPS of NiCoV$_{1.0}$-LDH/NF-100 at different reaction time in UOR.
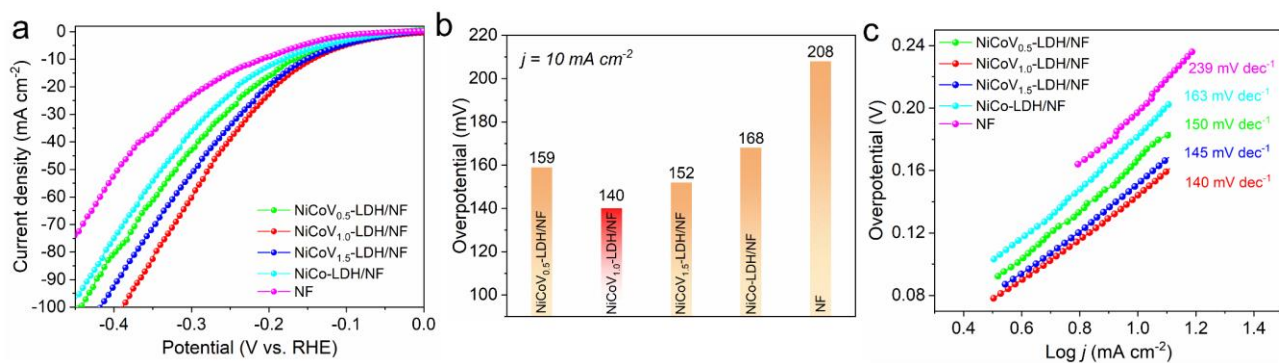
Fig. S18 (a) HER polarization curves, (b) comparison of overpotentials at 10 mA cm^{-2}, (c) Tafel slopes of NiCoV$_x$-LDH/NF (x = 0.5, 1.0, 1.5), NiCo-LDH/NF and NF.
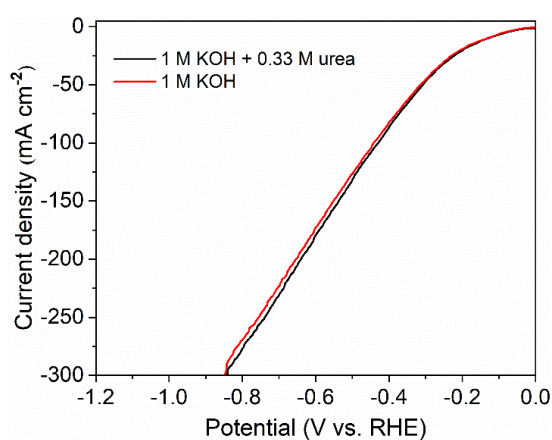
Fig. S19 The HER polarization curves of NiCoV$_{1.0}$-LDH/NF-100 in 1 M KOH and 1 M KOH +0.33 M urea were compared.
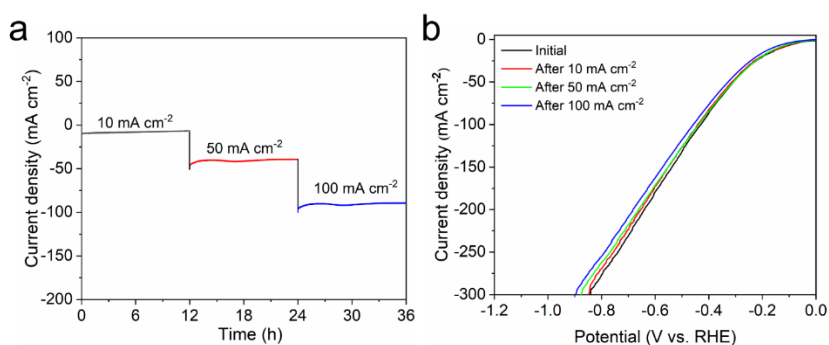
Fig. S20 (a) HER stability test and (b) LSV comparison before and after stability test of NiCoV$_{1.0}$-LDH/NF-100 composite.
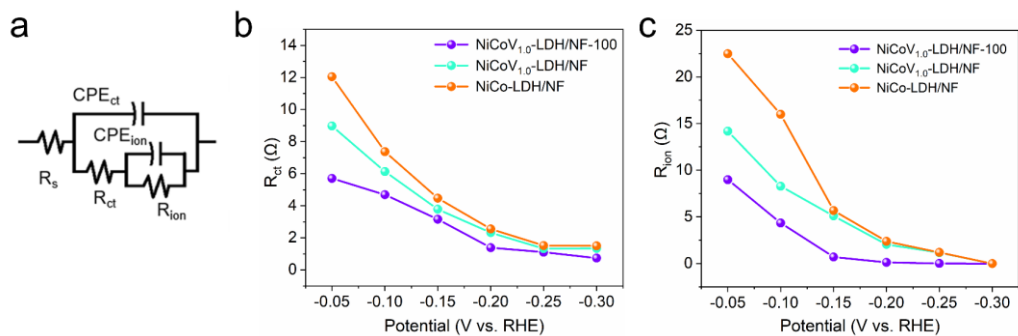
Fig. S21 (a) Equivalent circuit used for modeling the measured electrochemical response; (b, c) the R_{ct} and R_{ion} values of various catalysts at different voltages according to the fitted data of EIS.
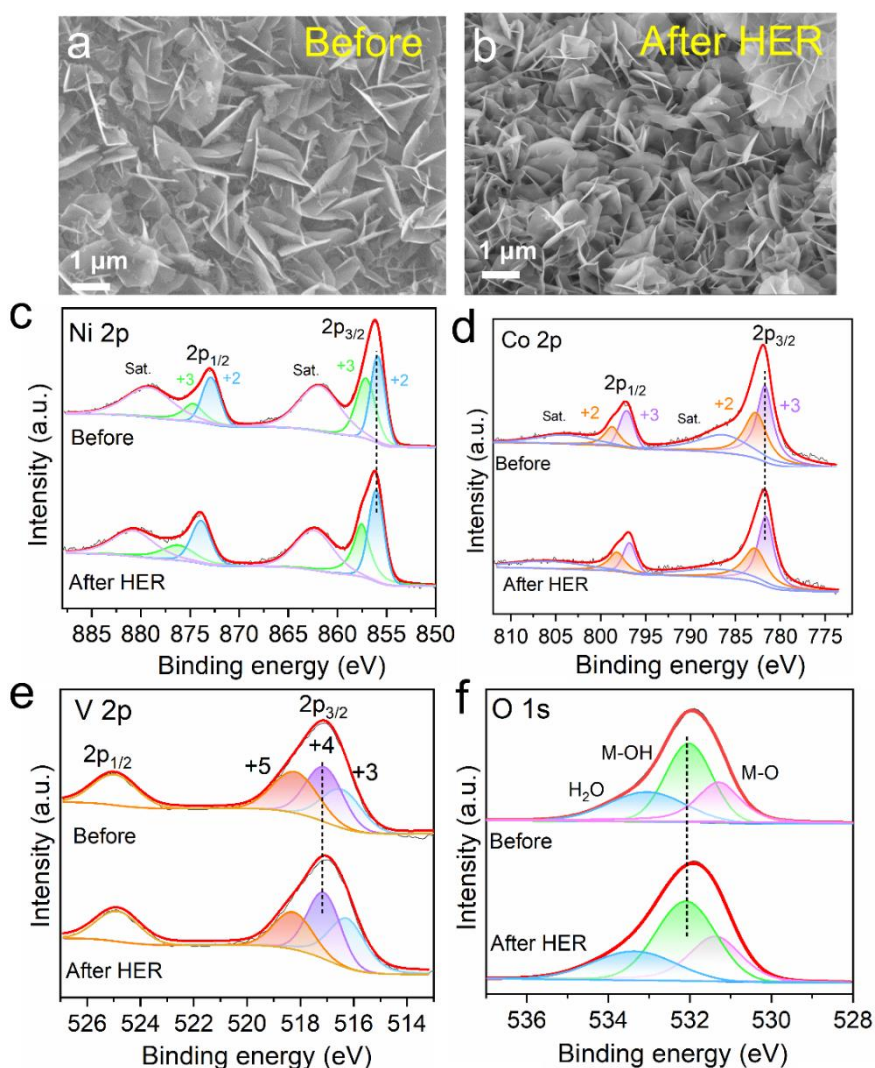
Fig. S22 (a-b) SEM comparison of NiCoV$_{1.0}$-LDH/NF-100 composite before and after HER reaction. (c-f) Ni 2p, Co 2p, V 2p, C 1s and O 1s XPS spectra of NiCoV$_{1.0}$-LDH/NF-100 before and after HER stability.
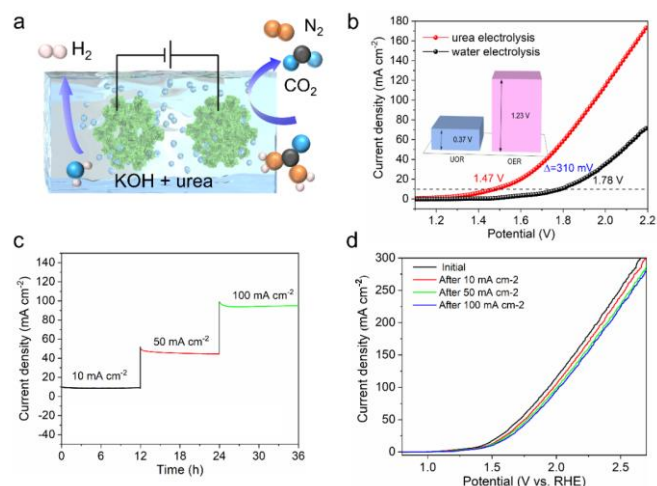
Fig. S23 (a) Schematic illustration of urea-assisted water electrolysis using NiCoV$_{1.0}$-LDH/NF-100 as bifunctional electrodes; (b) comparison of polarization curves of NiCoV$_{1.0}$-LDH/NF-100 during urea-assisted water electrolysis and water electrolysis; (c-d) stability test of NiCoV$_{1.0}$-LDH/NF-100 electrode in urea-assisted electrolysis water and comparison of LSV curves before and after stability test.
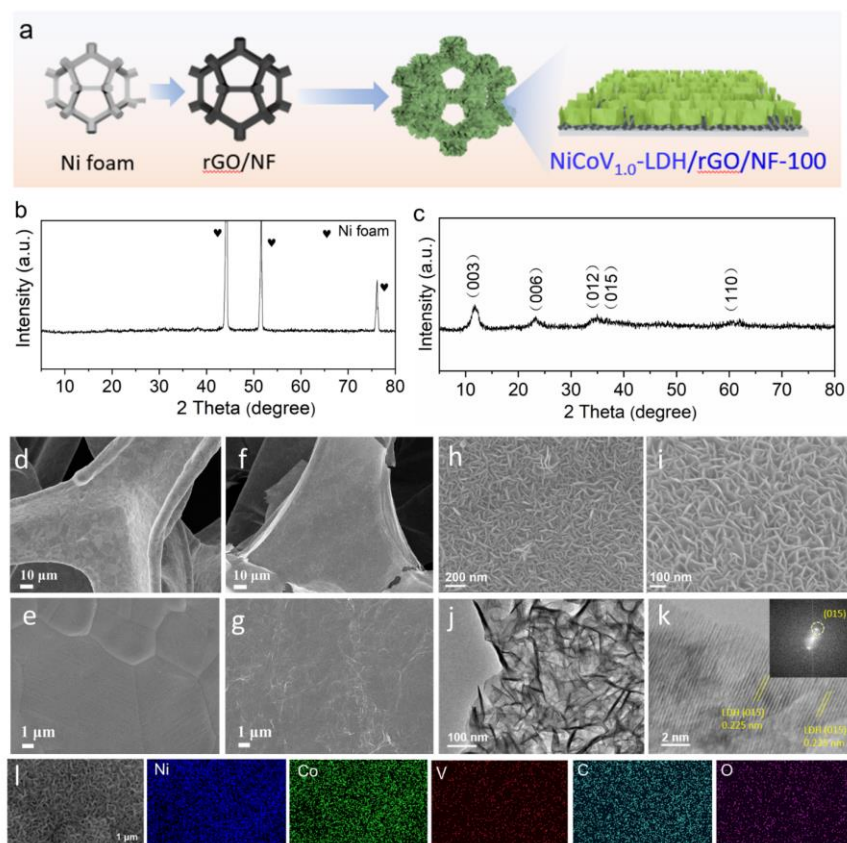
Fig. S24 (a) Synthesis strategy schematic of NiCoV$_{1.0}$-LDH/rGO/NF-100 with nanosheet array morphology; (b, c) XRD patterns of NiCoV$_{1.0}$-LDH/rGO/NF-100 and corresponding scraped powder sample. SEM images of NF (d, e) and rGO/NF (f, g). SEM (h, i), (HR)TEM (j, k) and SEM-EDX elemental mapping images (l) of NiCoV$_{1.0}$-LDH/rGO/NF-100.
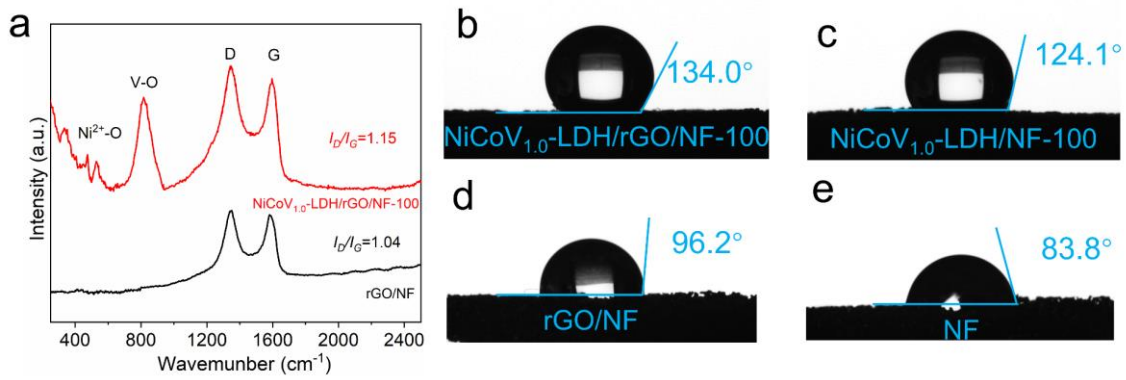
Fig. S25 (a) Raman spectra of NiCoV$_{1.0}$-LDH/rGO/NF-100 and rGO/NF. (b-c) Contact angles of NiCoV$_{1.0}$-LDH/rGO/NF-100, NiCoV$_{1.0}$-LDH/NF-100, rGO/NF and NF.
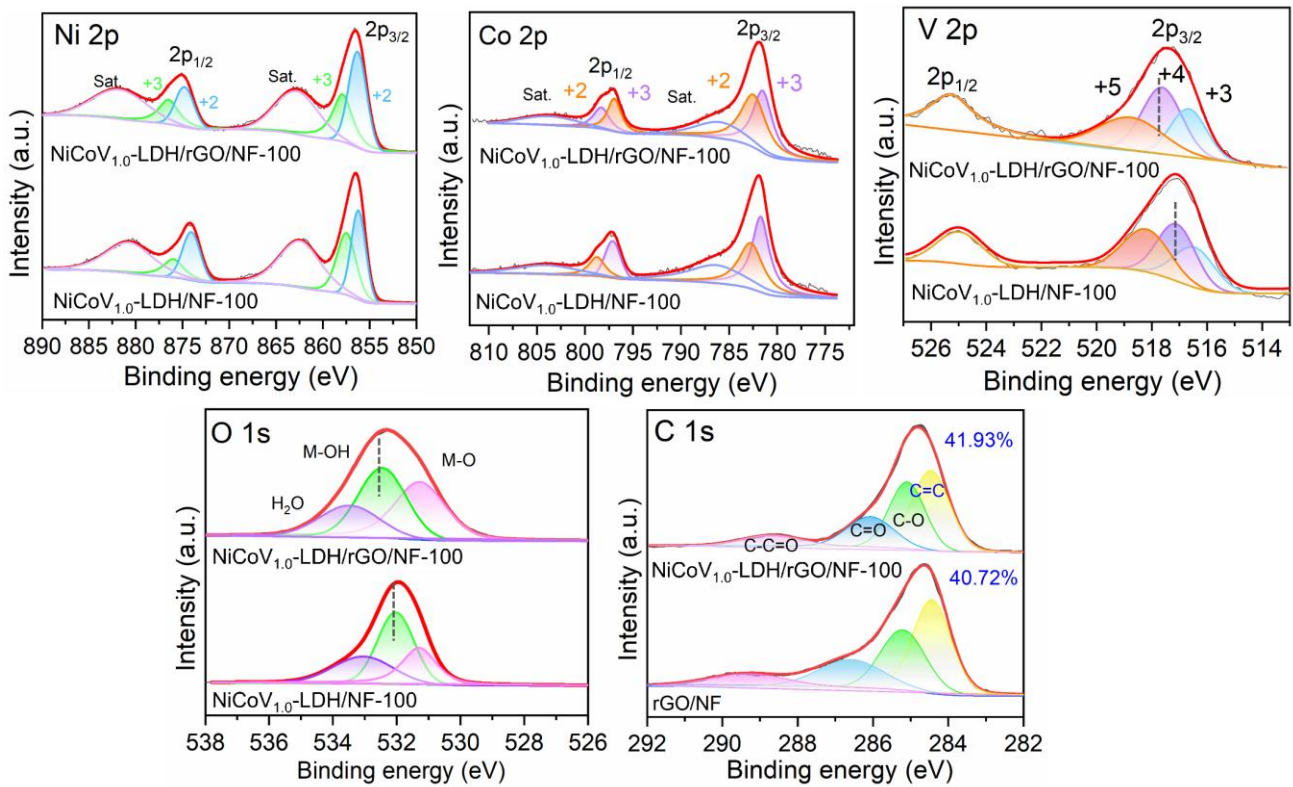
Fig. S26 XPS spectra of NiCoV$_{1.0}$-LDH/rGO/NF-100, NiCoV$_{1.0}$-LDH/NF-100 and rGO/NF.
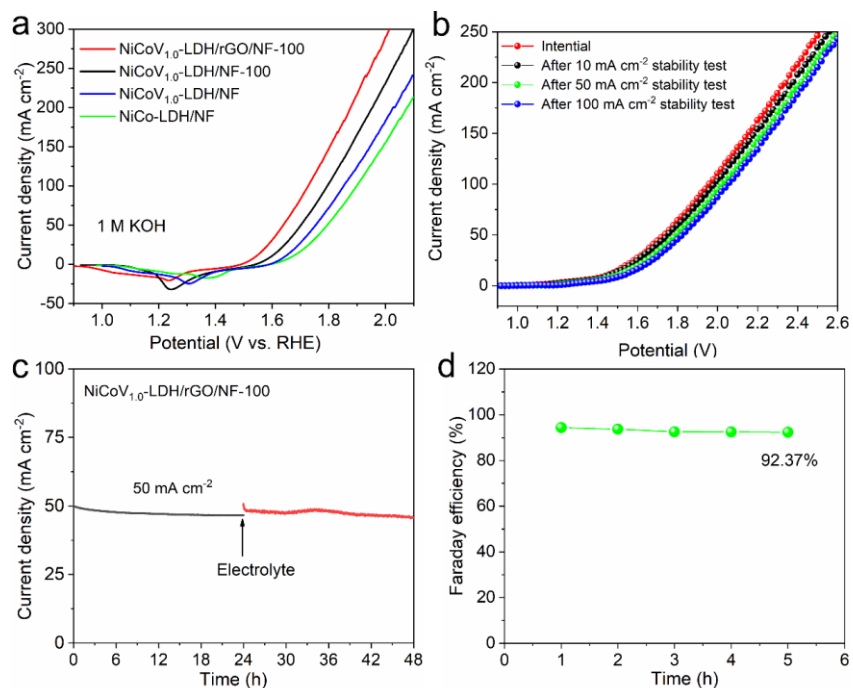
Fig. S27 (a) OER polarization curve of $NiCoV_{1.0}$-LDH/rGO/NF-100, $NiCoV_{1.0}$-LDH/NF-100, $NiCoV_{1.0}$-LDH/NF, and NiCo-LDH/NF. (b) Comparison of LSV curves before and after stability test of $NiCoV_{1.0}$-LDH/rGO/NF-100. (c) Stability before and after electrolyte replacement of $NiCoV_{1.0}$-LDH/rGO/NF-100. (d) Faradaic efficiency of H_2 production assisted by urea electrocatalysis system upon operation time at 50 mA cm^{-2}.
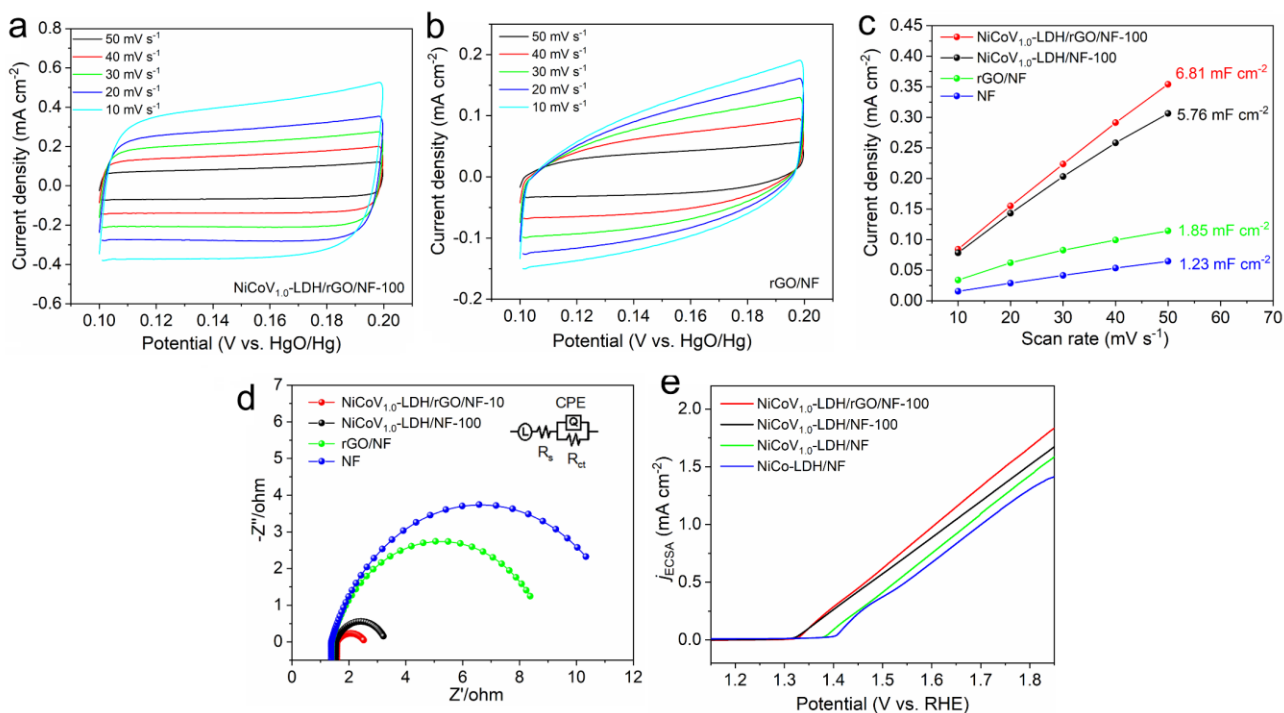
Fig. S28 (a-b) Cyclic voltammetry curves of $NiCoV_{1.0}$-LDH/rGO/NF-100 and rGO/NF at various scan rates in the region of 0.1-0.2 V vs. Hg/HgO. (c) The capacitive current densities of $NiCoV_{1.0}$-LDH/rGO/NF-100, $NiCoV_{1.0}$-LDH/NF-100, rGO/NF and bare NF plotted against different scan rates. (d) Nyquist plots of $NiCoV_{1.0}$-LDH/rGO/NF-100, $NiCoV_{1.0}$-LDH/NF-100, rGO/NF and bare NF during UOR process, the inset is the corresponding equivalent circuit. (e) ECSA normalized LSV curves of $NiCoV_{1.0}$-LDH/rGO/NF-100, $NiCoV_{1.0}$-LDH/NF-100, $NiCoV_{1.0}$-LDH/NF and NiCo-LDH/NF.
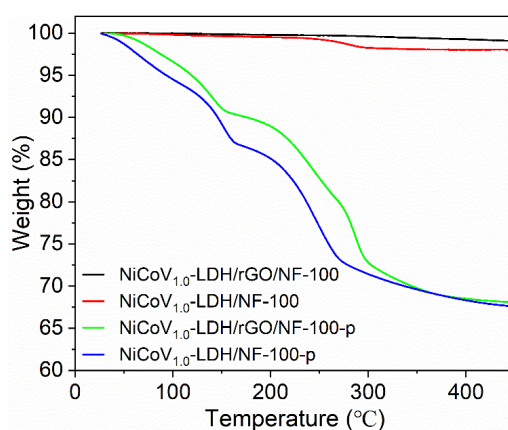
Fig. S29 TGA plots of $NiCoV_{1.0}$-LDH/rGO/NF-100, $NiCoV_{1.0}$-LDH/NF-100 and corresponding pure LDH, the suffix "p" stands for LDH precipitate formed during the synthesis of $NiCoV_{1.0}$-LDH/rGO/NF-100-p, which is named in the same way.
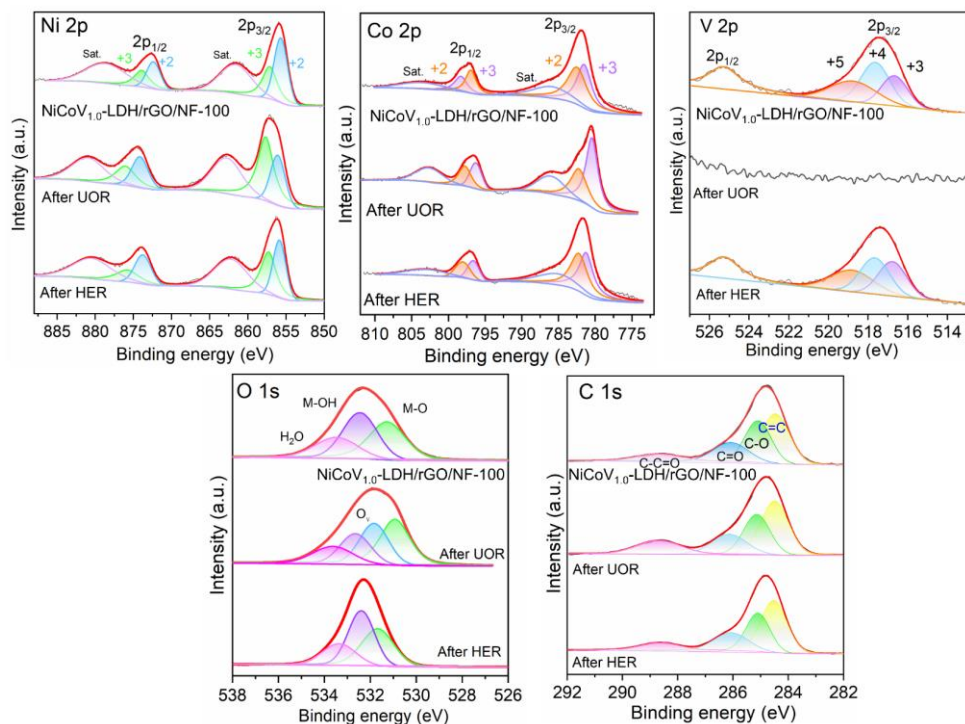
Fig. S30 Ni 2p, Co 2p, V 2p, C 1s and O 1s XPS spectrums of NiCoV$_{1.0}$-LDH/rGO/NF-100 composite before and after the chronoamperometry measurement.
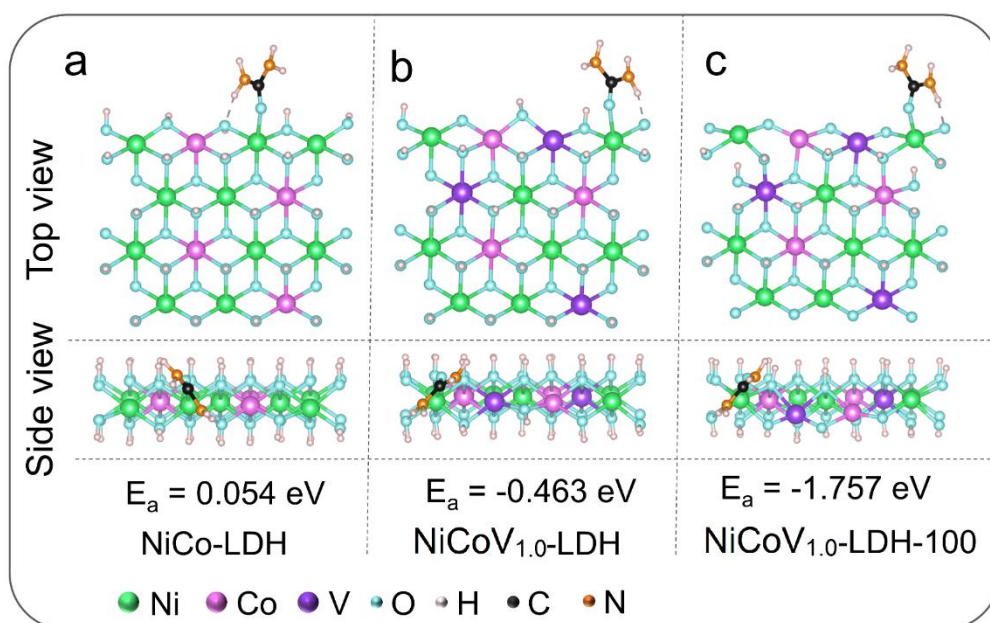
Fig. S31 Adsorption structure model of urea molecule at Ni metal sites in (a) NiCo-LDH, (b) NiCoV$_{1.0}$-LDH and (c) NiCoV$_{1.0}$-LDH-100.
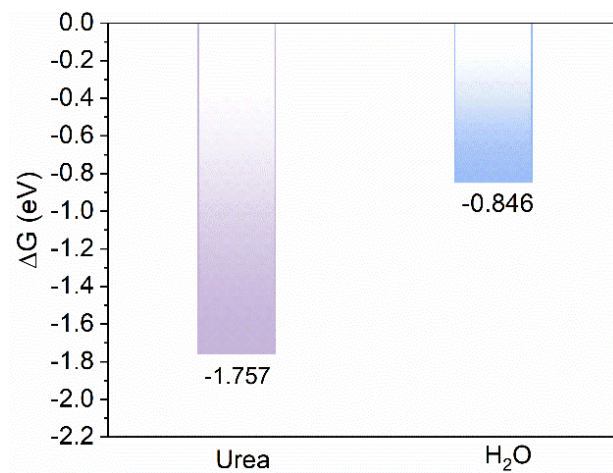
Fig. S32 Comparison of adsorption energies of urea and water molecules on NiCoV$_{1.0}$-LDH-100 catalyst.
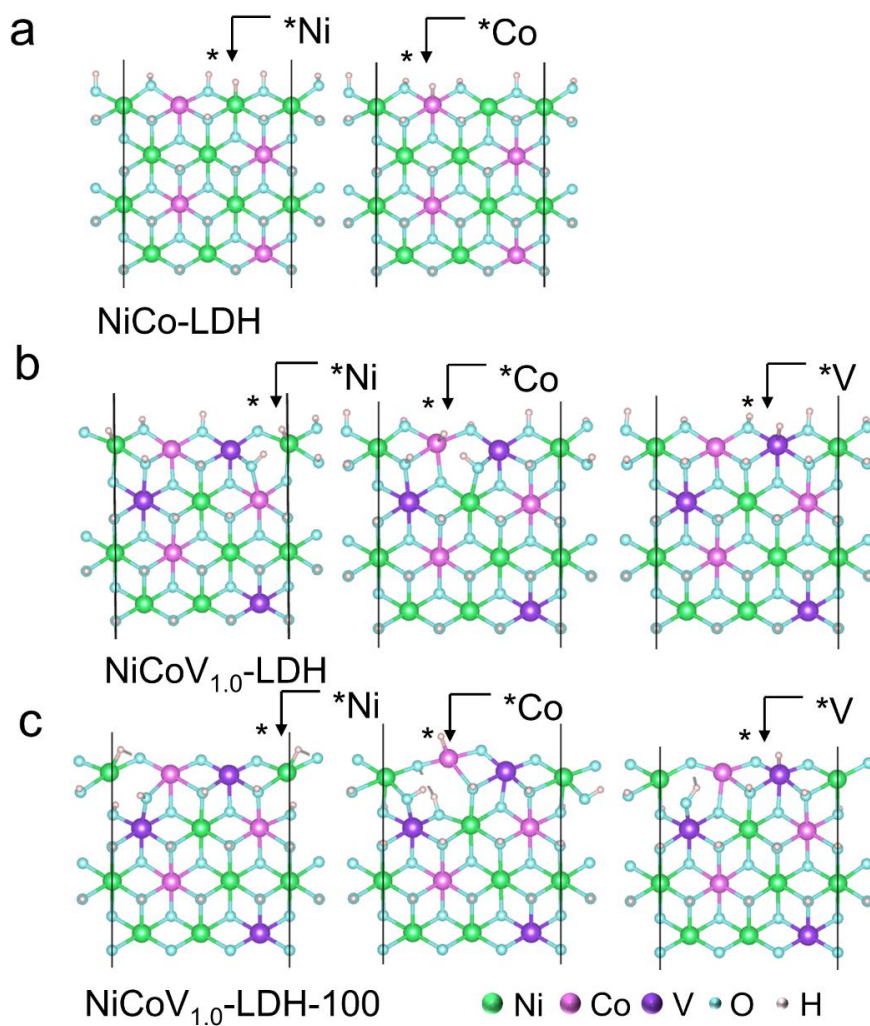
Fig. S33 Adsorption structure model of H atom at all metal sites (Ni, Co and V) in (a) NiCo-LDH, (b) NiCoV$_{1.0}$-LDH and (c) NiCoV$_{1.0}$-LDH-100.
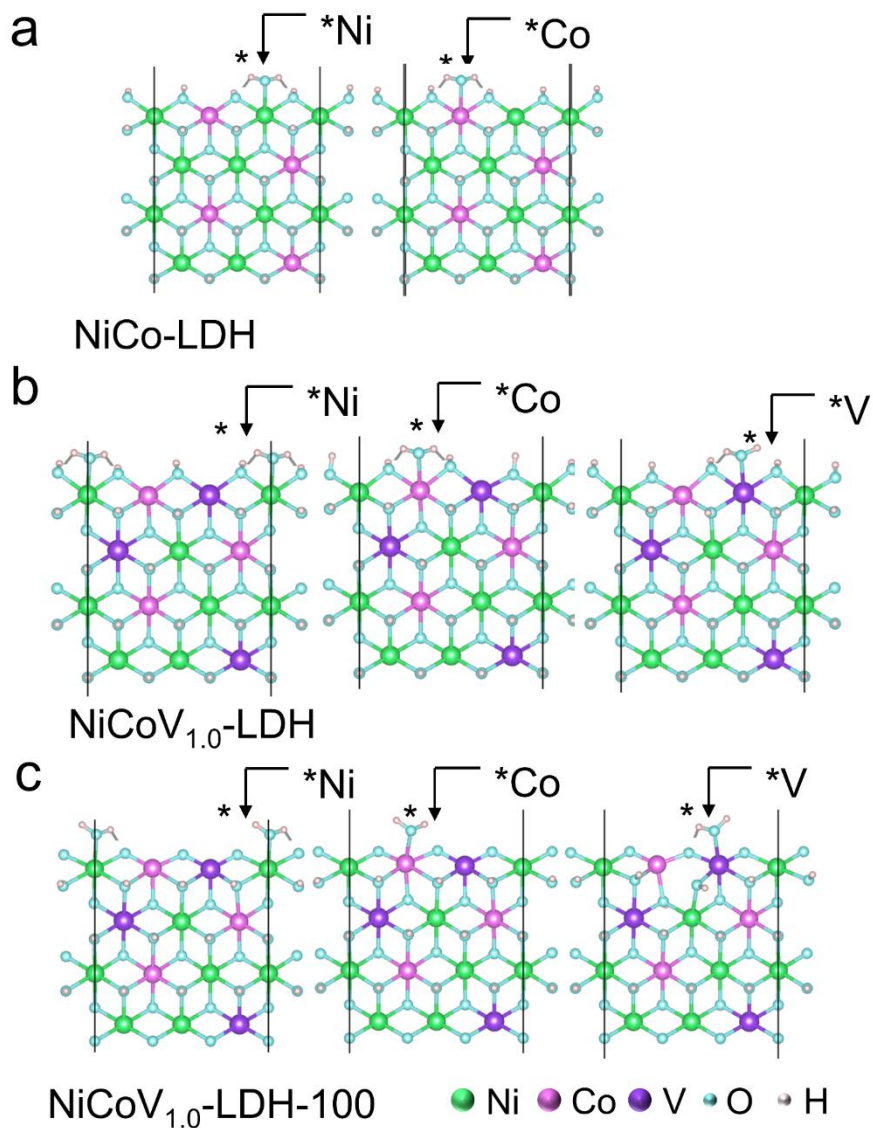
Fig. S34 Adsorption structure model of H_2O molecule at all metal sites (Ni, Co and V) in (a) NiCo-LDH, (b) $NiCoV_{1.0}$-LDH and (c) $NiCoV_{1.0}$-LDH-100.
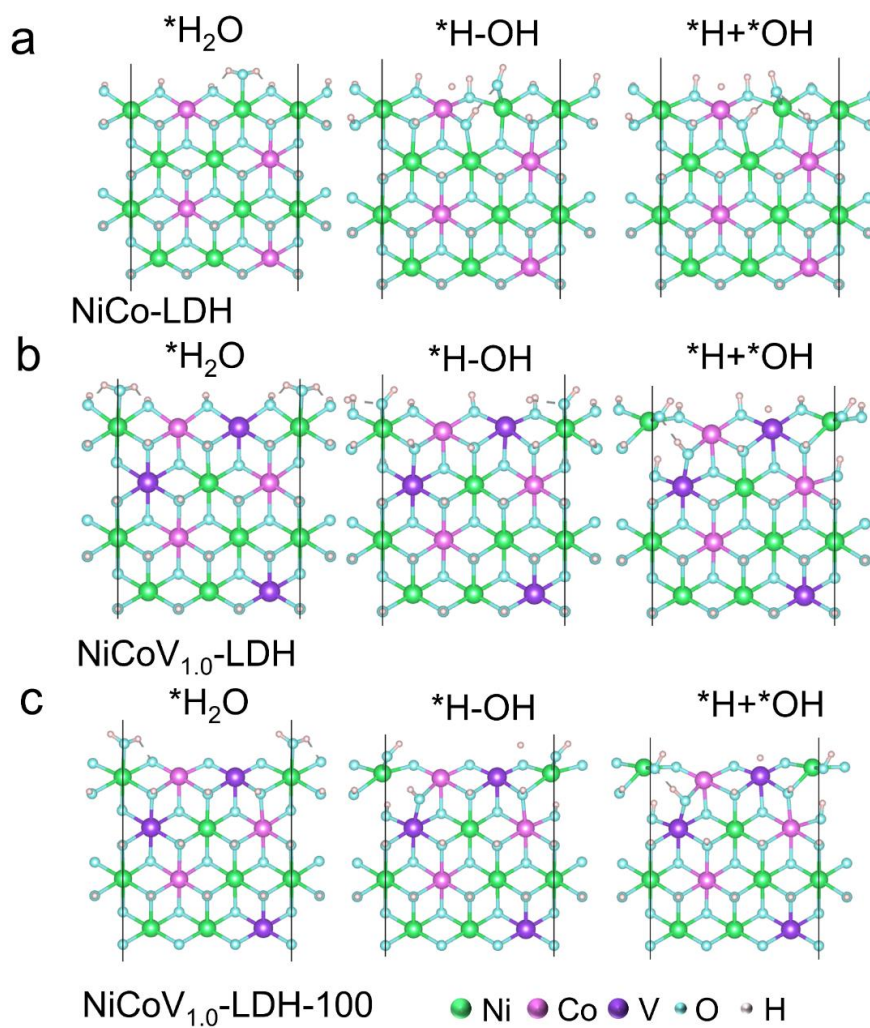
Fig. S35 Transition barrier model for H_2O dissociation of (a) NiCo-LDH, (b) $NiCoV_{1.0}$-LDH and (c) $NiCoV_{1.0}$-LDH-100.

Table S1. XRD parameters and ICP data for the NiCoV$_{1.0}$-LDH/NF-*y* (*y* = 50, 100, 200), NiCoV$_x$-LDH/NF (*x* = 0.5, 1.0, 1.5) and NiCo-LDH/NF composites.

Samples	d$_{003}$ (nm)	c (nm)[a]	D$_{003}$ (nm) [b]	Ni/Co/V ratio（ICP）
NiCoV$_{1.0}$-LDH/NF-50	0.7677	2.3031	14.09	2.26:1.01:0.80
NiCoV$_{1.0}$-LDH/NF-100	0.7674	2.3022	13.92	2.32:0.92:0.76
NiCoV$_{1.0}$-LDH/NF-200	0.7631	2.2893	12.65	2.13:0.95:0.81
NiCoV$_{1.5}$-LDH/NF	0.7651	2.2953	14.35	2.14:1.02:1.45
NiCoV$_{1.0}$-LDH/NF	0.7684	2.3052	15.35	2.21:0.92:0.85
NiCoV$_{0.5}$-LDH/NF	0.7702	2.3106	16.98	2.17:0.98:0.52
NiCo-LDH/NF	0.7604	2.2512	16.65	2.03:1.09

[a] Based on hexagonal system, c = 3d$_{003}$; [b] based on Scherrer equation, $D_{hkl} = k\lambda/(\beta\cos\theta)$, k = 0.89, λ = 0.1542 nm, β is the full width half maximum of the diffraction peak (rad.), θ is Bragg angle (º).

Table S2. The calculated ratios of Ni^{3+}/Ni^{2+}, Co^{3+}/Co^{2+}, $V^{4+}/(V^{3+} + V^{4+} + V^{5+})$ in $NiCoV_{1.0}$-LDH/NF-y (y = 50, 100, 200), $NiCoV_{1.0}$-LDH/NF, NiCo-LDH/NF composites.

（A）Samples	Ni $2p_{3/2}$ /eV		Ni $2p_{1/2}$ /eV		Ni^{3+}/Ni^{2+}
	Ni^{3+} (area)	Ni^{2+} (area)	Ni^{3+} (area)	Ni^{2+} (area)	ratio
$NiCoV_{1.0}$-LDH/NF-50	857.82 (40075)	856.30 (103104)	875.09 (36734)	873.73 (32309)	0.38
$NiCoV_{1.0}$-LDH/NF-100	857.87 (42878)	856.33 (103879)	875.98 (22902)	874.05 (50774)	0.41
$NiCoV_{1.0}$-LDH/NF-200	857.04 (37041)	855.54 (93034)	875.01 (39108)	873.27 (34998)	0.39
$NiCoV_{1.0}$-LDH/NF	857.52 (36775)	856.26 (99482)	575.60 (62873)	873.95 (35633)	0.37
NiCo-LDH/NF	856.99 (27594)	855.27 (122472)	874.40 (34136)	873.20 (42388)	0.23

（B）Samples	Co $2p_{3/2}$ /eV		Co $2p_{1/2}$ /eV		Co^{3+}/Co^{2+}
	Co^{3+} (area)	Co^{2+} (area)	Co^{3+} (area)	Co^{2+} (area)	ratio
$NiCoV_{1.0}$-LDH/NF-50	781.60 (22381)	782.31 (23674)	797.10 (6003)	798.42 (9133)	0.94
$NiCoV_{1.0}$-LDH/NF-100	781.70 (33416)	782.73 (29574)	797.11 (10995)	798.73 (8389)	1.13
$NiCoV_{1.0}$-LDH/NF-200	781.02 (32607)	782.24 (35442)	796.38 (8834)	797.85 (7911)	0.92
$NiCoV_{1.0}$-LDH/NF	781.84 (23965)	782.56 (26379)	797.14 (8274)	798.65 (9542)	0.90
NiCo-LDH/NF	781.98 (25125)	782.33 (30495)	796.78 (6063)	798.30 (5259)	0.82

（C）Samples	V $2p_{3/2}$ /eV			V^{4+} / (V^{3+} + V^{4+} + V^{5+}) / %
	V^{3+} (area)	V^{4+} (area)	V^{5+} (area)	
$NiCoV_{1.0}$-LDH/NF-50	515.89 (1241)	516.80 (970)	517.80 (623)	34.22
$NiCoV_{1.0}$-LDH/NF-100	516.43 (1267)	517.08 (1692)	518.21 (1532)	37.61
$NiCoV_{1.0}$-LDH/NF-200	515.95 (1156)	517.08 (869)	518.41 (686)	32.05
$NiCoV_{1.0}$-LDH/NF	515.61 (2084)	516.63 (1390)	518.05 (975)	31.24

Table S3. The EAXFS fitting parameters and results of Ni and Co in NiCoV$_{1.0}$-LDH/NF-100, NiCoV$_{1.0}$-LDH/NF and NiCo-LDH/NF composites.

Samples	Shell	[a]C.N.	[b]R(Å)	[c]σ^2(Å^2)	ΔE_0(eV)[d]	S_0^2	[d]R-factor
NiCoV$_{1.0}$-LDH/NF-100	Ni-O	5.6 ± 0.3	2.05	0.006	-4.9 ± 0.4	0.8061	0.017
	Ni-Ni	5.1 ± 0.4	3.07	0.007			
	Co-O	6.0 ± 0.2	1.97	0.012	-5.7 ± 0.3	0.8052	0.005
	Co-Ni	0.2 ± 0.1	2.49	0.001			
	Co-Co	5.1 ± 0.3	3.06	0.010			
	Co-V	0.3 ± 0.2	2.31	0.018			
NiCoV$_{1.0}$-LDH/NF	Ni-O	6.0 ± 0.3	2.05	0.006	-5.9 ± 0.4	0.8061	0.017
	Ni-Ni	5.2 ± 0.4	3.08	0.007			
	Co-O	6.0 ± 0.4	1.98	0.012	-2.8 ± 0.5	0.8052	0.019
	Co-Ni	1.1 ± 0.4	2.49	0.010			
	Co-Co	5.5 ± 0.4	3.08	0.009			
	Co-V	0.9 ± 0.2	2.31	0.007			
NiCo-LDH/NF	Ni-O	6.0 ± 0.2	2.05	0.006	-2.3 ± 0.3	0.8061	0.014
	Ni-Ni	6.0 ± 0.4	3.07	0.010			
	Co-O	5.9 ± 0.2	2.04	0.011	-2.0 ± 0.3	0.8052	0.010
	Co-Ni	5.2 ± 0.3	3.10	0.011			
	Co-Co	1.1 ± 0.4	3.43	0.020			

[a] C.N.: coordination number; [b] R: bond distance; [c] σ^2: Debye-Waller factor; [d] R-factor (%): if r < 5％, consistent with broadly correct models.

Table S4. EIS fitting parameters from equivalent circuits of NiCoV$_{1.0}$-LDH/NF-100 composite during OER process.

Potential (V vs. RHE)	Impedimetric parameters (1 M KOH)				
	L (H cm^{-2})	R$_s$ (Ω cm^{-2})	Q-Y$_o$ (S s^n cm^{-2})	Q-n	R$_{ct}$ (Ω cm^{-2})
1.10 V	8.789*10^{-7}	1.559	0.002403	0.7584	3.760*10^{-13}
1.20 V	8.536*10^{-7}	1.667	0.0106	0.769	8.098*10^{-4}
1.30 V	8.797*10^{-7}	1.597	0.02118	0.7123	2.374*10^{-4}
1.35 V	9.342*10^{-7}	1.556	0.9751	0.7456	2.374*10^{-8}
1.40 V	8.925*10^{-7}	1.634	0.6173	0.6295	1.296*10^{-10}
1.45 V	9.176*10^{-7}	1.577	0.7677	0.7742	3.673*10^{-8}
1.50 V	9.261*10^{-7}	1.561	0.5455	0.7235	22.56
1.55 V	9.319*10^{-7}	1.546	0.4507	0.6526	3.38
1.60 V	9.335*10^{-7}	1.542	0.4188	0.6332	0.7115
1.65 V	9.305*10^{-7}	1.538	0.3698	0.6276	0.3722

Table S5. EIS fitting parameters from equivalent circuits of NiCoV$_{1.0}$-LDH/NF-100 composite during UOR process.

Potential (V vs. RHE)	Impedimetric parameters (1 M KOH + 0.33 M Urea)				
	L (H cm^{-2})	R$_s$ (Ω cm^{-2})	Q-Y$_o$ (S s^n cm^{-2})	Q-n	R$_{ct}$ (Ω cm^{-2})
1.10 V	8.622*10^{-7}	1.583	0.001496	0.8101	3.231*10^{-13}
1.20 V	8.789*10^{-7}	1.559	0.002403	0.7584	3.76*10^{-13}
1.25V	8.712*10^{-7}	1.569	0.004329	0.7219	1.616*10^{-17}
1.30V	8.604*10^{-7}	1.585	0.008196	0.6966	1.812*10^{-17}
1.35 V	8.635*10^{-7}	1.578	0.01693	0.6667	18.680
1.40 V	8.550*10^{-7}	1.607	0.2987	0.7167	8.817
1.45 V	9.211*10^{-7}	1.536	0.3887	0.7163	1.770
1.50 V	9.307*10^{-7}	1.517	0.4426	0.6335	1.118
1.55 V	9.284*10^{-7}	1.512	0.4342	0.6087	0.9495
1.60 V	9.335*10^{-7}	1.515	0.4585	0.5974	0.9172
1.65 V	9.344*10^{-7}	1.507	0.5619	0.5326	1.270

Table S6. EIS fitting parameters from equivalent circuits of NiCoV$_{1.0}$-LDH/NF-y (y = 50, 100, 200), NiCoV$_{1.0}$-LDH/NF, NiCo-LDH/NF and NF during UOR process at 1.45 V.

Electrocatalysts	Impedimetric parameters (1 M KOH + 0.33 M Urea)				
	L (H cm^{-2})	R_s (Ω cm^{-2})	Q-Y$_o$ (S s^n cm^{-2})	Q-n	R_{ct} (Ω cm^{-2})
NiCoV$_{1.0}$-LDH/NF-50	1.042*10^{-6}	1.382	0.1950	0.8037	3.071
NiCoV$_{1.0}$-LDH/NF-100	9.211*10^{-7}	1.536	0.3887	0.7163	1.770
NiCoV$_{1.0}$-LDH/NF-200	1.048*10^{-6}	1.389	0.1870	0.7920	5.193
NiCoV$_{1.0}$-LDH/NF	1.047*10^{-6}	1.391	0.1965	0.7894	5.795
NiCo-LDH/NF	1.046*10^{-6}	1.389	0.2001	0.7900	7.681
NF	1.051*10^{-6}	1.382	0.2192	0.7891	10.490

Table S7. The Ni^{3+}/Ni^{2+} and Co^{3+}/Co^{2+} ratio of the NiCoV$_{1.0}$-LDH/NF-100 composite before and after the UOR reaction.

Samples	Ni 2p$_{3/2}$/eV		Ni 2p$_{1/2}$/eV		Ni^{3+}/Ni^{2+} ratio
	Ni^{3+} (area)	Ni^{2+} (area)	Ni^{3+} (area)	Ni^{2+} (area)	
Initial	857.47 (78540)	856.21 (77312)	875.98 (31719)	874.05 (50774)	0.41
After UOR	856.63 (38930)	855.25 (22086)	874.55 (15094)	874.05 (13050)	1.76

Samples	Co 2p$_{3/2}$/eV		Co 2p$_{1/2}$/eV		Co^{3+}/Co^{2+} ratio
	Co^{3+} (area)	Co^{2+} (area)	Co^{3+} (area)	Co^{2+} (area)	
Initial	781.70 (36394)	782.73 (29574)	797.11 (10995)	798.73 (8389)	1.13
After UOR	781.04 (7476)	782.23 (3413)	796.20 (2991)	797.49 (2016)	2.19

Table S8. The fitted parameters of the EIS data of NiCoV$_{1.0}$-LDH/NF-100, NiCoV$_{1.0}$-LDH/NF and NiCo-LDH/NF composites (1 M KOH).

Catalysts	Potential (V vs. RHE)	R_s (Ω)	CPE (F S^{n-1})	R_{ct} (Ω)	C_φ (F)	R_{ion} (Ω)
NiCoV$_{1.0}$-LDH/NF-100	-0.05	1.750	0.0003716	4.686	0.001003	8.988
	-0.10	1.737	0.0003479	3.154	0.0009297	4.347
	-0.15	1.728	0.0002777	1.384	0.0005291	0.7081
	-0.20	1.733	0.0002939	1.103	0.001573	0.1305
	-0.25	1.744	0.0003057	0.7393	0.005761	0.01264
	-0.30	1.746	0.0003202	0.4364	$3.65*10^{-8}$	$2.476*10^{-8}$
NiCoV$_{1.0}$-LDH/NF	-0.05	1.647	0.0001092	8.974	0.0003655	14.18
	-0.10	1.658	0.0005513	6.135	0.001696	8.276
	-0.15	1.652	0.0003053	3.782	0.0006576	5.106
	-0.20	1.606	0.0004089	2.324	0.0006958	2.056
	-0.25	1.620	0.0003061	1.327	0.0004959	1.172
	-0.30	1.610	0.0004193	1.341	0.0009535	$1.158*10^{-6}$
NiCo-LDH/NF	-0.05	1.610	0.0002124	12.050	0.0007333	22.48
	-0.10	1.616	0.0002626	7.370	0.001017	15.98
	-0.15	1.582	0.0003874	4.474	0.001314	5.684
	-0.20	1.561	0.0003842	2.552	0.001088	2.378
	-0.25	1.551	0.0003632	1.523	0.000902	1.197
	-0.30	1.562	0.0004044	1.499	0.0008086	$4.435*10^{-6}$

Table S9. EIS fitting parameters from equivalent circuits of NiCoV$_{1.0}$-LDH/rGO/NF-100, NiCoV$_{1.0}$-LDH/NF-100, rGO/NF and NF during UOR process.

Electrocatalysts	Impedimetric parameters (1 M KOH + 0.33 M urea)				
	L (H cm^{-2})	R_s (Ω cm^{-2})	Q-Y$_o$ (S s^n cm^{-2})	Q-n	R_{ct} (Ω cm^{-2})
NiCoV$_{1.0}$-LDH/rGO/NF-100	$1.128*10^{-6}$	1.574	0.1691	0.5556	1.142
NiCoV$_{1.0}$-LDH/NF-100	$9.211*10^{-7}$	1.536	0.3887	0.7163	1.77
rGO/NF	$9.668*10^{-7}$	1.491	0.0016	0.84	10.93
NF	$1.051*10^{-6}$	1.382	0.2192	0.7891	10.49

Table S10. Comparison of the electrocatalytic UOR activity (1.0 M KOH) between the $NiCoV_{1.0}$-LDH/rGO/NF-100 composite and other catalysts.

Catalysts	[Urea]/M	Performance/V @mA cm^{-2}	Tafel slope/mV dec^{-1}	Refs.
$NiCoV_{1.0}$-LDH/rGO/NF-100	**0.33 M**	**1.33@10**	**32**	**This work**
$NiCoV_{1.0}$-LDH/NF-100	**0.33 M**	**1.35@10**	**34**	
FQD/CoNi LDH/NF	0.5 M	1.36@10	17	[5]
NiMoV LDH/NF	0.33 M	1.40@100	24.29	[6]
NiFeCo LDH/NF	0.33 M	1.49@10	31	[7]
$Co_2(OH)_3Cl$-V-n	0.33 M	1.54@30	135.3	[8]
NiAl-LDHs/CFP	0.33 M	1.42@10	59.8	[9]
$Ni(OH)_2$@NF	0.33 M	1.35@10	24.37	[10]
Rh/NiV-LDH	0.33 M	1.33@10	36	[11]
V-$Ni(OH)_2$	0.33 M	1.33@10	32.15	[12]
Co, V co-doped NiS_2	0.33 M	1.35@10	30.31	[13]
Ni/FeOOH	0.5 M	1.37@10	26	[14]
Ni-Mo nanotube	0.1 M	1.43@10	22	[15]
CoMn/$CoMn_2O_4$	0.5 M	1.51@100	38	[16]
NF/NiMoO-Ar	0.5 M	1.37@10	19	[17]
Ni-S-Se/NF	0.5 M	1.38@10	28	[18]
O-NiMoP/NF	0.5 M	1.41@100	34	[19]

Table S11. Comparison of the electrocatalytic HER activity between the $NiCoV_{1.0}$-LDH/rGO/NF-100 composite and other recently reported catalysts.

Electrocatalysts	Substrate	Method	HER/mV	Ref.
$NiCoV_{1.0}$-LDH/rGO/NF-100	**Ni foam**	**hydrothermal**	**70 (η_{10})**	**This work**
$NiCoV_{1.0}$-LDH/NF-100	**Ni foam**	**hydrothermal**	**80 (η_{10})**	
Co_3Fe_1-LDH/rGO/NF	Ni foam	co-precipitation	110 (η_{10})	[1]
Ni_2Fe_1-LDH/rGO/NF	Ni foam	hydrothermal	109 (η_{10})	[2]
$Ni_6Fe_1Mo_1$-LDH/rGO/NF	Ni foam	hydrothermal	90 (η_{10})	[3]
FQD/CoNi-LDH/NF	Ni foam	hydrothermal	150 (η_{10})	[5]
NiFeCo LDH/NF	Ni foam	electrodeposition	108 (η_{10})	[7]
NiCo LDH-V_{Ni}/CC	Carbon cloth	hydrothermal and chemical etching	195 (η_{10})	[20]
NiMoCo-LDH	Ni foam	hydrothermal	123 (η_{10})	[21]
0.8 GO-FeNi-LDH	Ni foam	electrodeposition	119 (η_{10})	[22]
in-NiV-LDH/NF	Ni foam	hydrothermal	114 (η_{10})	[23]
CoMoV LDH/NF	Ni foam	hydrothermal	150 (η_{10})	[24]
NiFeW/CP	Carbon paper	electrodeposition	115 (η_{10})	[25]
NiCoMo-LDH	GCE	hydrothermal	93 (η_{10})	[26]
CoMo-LDH	Ni foam	co-precipitation	115 (η_{10})	[27]
CoMo-LDH	GCE	hydrothermal	325 (η_{100})	[28]
Ru/NiFe LDH-F/NF	Ni foam	hydrothermal	115.6 (η_{10})	[29]
NiFe-LDH@CoS_x/NF	Ni foam	hydrothermal and electrodeposition	143 (η_{10})	[30]

References

[1]   J. Guo, Z. Wei, K. Wang, H. Zhang, Int. J. Hydrogen Energy 2021, 46, 27529.

[2]   K. Wang, J. Guo, H. Zhang, Mater. Adv. 2022, 3, 6887.

[3]   J. Guo, K. Wang, H. Zhang, H. Zhang, ACS Appl. Nano Mater. 2023, 6, 379.

[4]   T. Brezesinski, J. Wang, J. Polleux, B. Dunn, S. H. Tolbert, J. Am. Chem. Soc. 2009, 131, 1802.

[5]   Y. Feng, X. Wang, J. Huang, P. Dong, J. Ji, J. Li, L. Cao, L. Feng, P. Jin, C. Wang, Chem. Eng. J. 2020, 390, 124525.

[6]   Z. Wang, W. Liu, J. Bao, Y. Song, X. She, Y. Hua, G. Lv, J. Yuan, H. Li, H. Xu, Chem. Eng. J. 2022, 430, 133100.

[7]   P. Babar, A. Lokhande, V. Karade, B. Pawar, M. G. Gang, S. Pawar, J. H. Kim, ACS Sustainable Chem. Eng. 2019, 7, 10035.

[8]   B. Zhang, C. Pan, H. Liu, X. Wu, H. Jiang, L. Yang, Z. Qi, G. Li, L. Shan, Y. Lin, L. Song, Y. Jiang, Chem. Eng. J. 2022, 439, 135768.

[9]   Y. Wang, Y. Liu, M. Zhang, B. Liu, Z. Zhao, K. Yan, Sci. China Mater. 2022, 65, 1805.

[10] L. Xia, Y. Liao, Y. Qing, H. Xu, Z. Gao, W. Li, Y. Wu, ACS Appl. Mater. Interfaces 2020, 3, 2996.

[11] H. Sun, L. Li, H. C. Chen, D. Duan, M. Humayun, Y. Qiu, X. Zhang, X. Ao, Y. Wu, Y. Pang, K. Huo, C. Wang, Y. Xiong, Sci. Bull. 2022, 67, 1763.

[12] Q. Cao, Y. Yuan, K. Wang, W. Huang, Y. Zhao, X. Sun, R. Ding, W. Lin, E. Liu, P. Gao, J. Colloid Interface Sci. 2022, 618, 411.

[13] Z. Ji, Y. Song, S. Zhao, Y. Li, J. Liu, W. Hu, ACS Catal. 2022, 12, 569.

[14] J.-J. Zhang, W.-W. Bao, M.-Y. Li, C.-M. Yang, N.-N. Zhang, Chem. Commun. 2020, 56, 14713.

[15] J.-Y. Zhang, T. He, M. Wang, R. Qi, Y. Yan, Z. Dong, H. Liu, H. Wang, B. Y. Xia, Nano Energy 2019, 60, 894.

[16] C. Wang, H. Lu, Z. Mao, C. Yan, G. Shen, X. Wang, Adv. Funct. Mater. 2020, 30, 2000556.

[17] Z.-Y. Yu, C.-C. Lang, M.-R. Gao, Y. Chen, Q.-Q. Fu, Y. Duan, S.-H. Yu, Energy Environ. Sci. 2018, 11, 1890.

[18] N. Chen, Y.-X. Du, G. Zhang, W.-T. Lu, F.-F. Cao, Nano Energy 2021, 81, 105605.

[19] H. Jiang, M. Sun, S. Wu, B. Huang, C.-S. Lee, W. Zhang, Adv. Funct. Mater. 2021, 31, 2104951.

[20] W. He, D. Cao, D. Ma, Y. Li, C. Chen, L. Liang, H. Liu, Chem. Commun. 2022, 58, 7757.

[21] H. Liu, D. Zhao, Y. Liu, Y. Tong, X. Wu, G. Shen, Sci. China Mater. 2021, 64, 581.

[22] X. Han, N. Suo, C. Chen, Z. Lin, Z. Dou, X. He, L. Cui, Int. J. Hydrogen Energy 2019, 44, 29876.

[23] D. He, L. Cao, J. Huang, K. Kajiyoshi, J. Wu, C. Wang, Q. Liu, D. Yang, L. Feng, J. Energy Chem. 2020, 47, 263.

[24] J. Bao, Z. Wang, J. Xie, L. Xu, F. Lei, M. Guan, Y. Zhao, Y. Huang, H. Li, Chem. Commun. 2019, 55, 3521.

[25] L. Ding, K. Li, Z. Xie, G. Yang, S. Yu, W. Wang, H. Yu, J. Baxter, H. M. Meyer, D. A. Cullen, F.-Y. Zhang, ACS Appl. Mater. Interfaces 2021, 13, 20070.

[26] S. M. N. Jeghan, N. Kim, G. Lee, Int. J. Hydrogen Energy 2021, 46, 22463.

[27] J. Bao, Z. Wang, J. Xie, L. Xu, F. Lei, M. Guan, Y. Huang, Y. Zhao, J. Xia, H. Li, Inorg. Chem. Front. 2018, 5, 2964.

[28] S. M. N. Jeghan, J. Kim, G. Lee, Appl. Surf. Sci. 2021, 546, 149072.

[29] Y. Wang, P. Zheng, M. Li, Y. Li, X. Zhang, J. Chen, X. Fang, Y. Liu, X. Yuan, X. Dai, H. Wang, Nanoscale 2020, 12, 9669.

[30] Y. Yang, Y. Xie, Z. Yu, S. Guo, M. Yuan, H. Yao, Z. Liang, Y. R. Lu, T.-S. Chan, C. Li, H. Dong, S. Ma, Chem. Eng. J. 2021, 419, 129512.